Energy 332 (2025) 137209

Contents lists available at ScienceDirect

Energy

journal homepage: www.elsevier.com/locate/energy

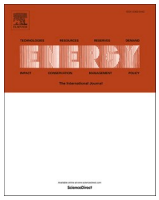

An innovative experimental pilot-plant to investigate the gasification process of biomass impact of raw and torrefied pellet on the process performances

M. Grigiante [a,*], D. Antolini [b]

[a] Department of Civil, Environmental and Mechanical Engineering, University of Trento, Via Mesiano 77, 38123, Trento, Italy
[b] BiSTEMS srl, NOI Techpark, via Alessandro Volta 13/A, 39100, Bolzano, Italy

ARTICLE INFO

Handling Editor: Wojciech Stanek

ABSTRACT

In this paper the results of an experimental study on gasification process are presented. A small batch reactor, using air as gasification agent, has been suitable designed to investigate the gasification of both raw and torrefied biomass (*spruce*) densified in form of pellet (*P*). The novelty of this study consists in the continuous monitoring of the biomass lost amount (gasified biomass) by placing the reactor, appropriately instrumented, on a suitable scale. Thanks to this simple expedient, it has been possible to rework the mass and energy balances of the process as if they accord to those of a continuous steady-state updraft fixed-bed configuration. The experimental results have been processed by elaborating a dedicated procedure that has allowed to turn the quantities expressed in term of mass amount, such as the treated biomass and the char production, into mass flow rate quantities. This study highlights the role of the air flow rate $\dot{V}_{a,wb}$ as guiding parameter through which the performance indexes of the process as *cold gasification* (η_C) and *carbon conversion* (η_{CC}) *efficiencies*, *syngas* (Y_s) and *power to biomass* (Y_{pb}) *yields* can be assessed. Within the selected $\dot{V}_{a,wb}$ ranges: 15–25 Nl·min^{-1} for raw wood pellet (*WP*) and 15–30 Nl·min^{-1} for torrefied pellet (*TP*), the *reactor gasification power* (P_{gr}) sets within: 1,45-2,18 kW for *WP* and 1,66-3,23 kW for *TP*. Furthermore, the results demonstrate the fundamental role of the char layer in improving the quality of the Low Heating Value (*LHV*) of the produced syngas in turn also conditioned by the selected $\dot{V}_{a,wb}$ values. As general outcome, the performances results more promising for *TP* than *WP*. Both the experimental approach and the proposed elaboration procedure provide an alternative methodology that could contribute to improve the design procedures to enhance the exploitation of this technology within the current renewable energy scenarios.

Nomenclature

Abbreviation/Symbols		*Subscripts*	
MC	Moisture Content (%)	*a*	air
WP	Wood Pellets	*b*	biomass
TP	Torrefied Pellet	*bl*	biomass loss/lost
$\dot{m}$	mass flow rate [kg·h^{-1}]	*c*	cold gasification
$\dot{V}$	Volumetric flow rate [Nl·min^{-1}]	*cc*	carbon conversion
ρ	density [kg·m^{-3}]	*db*	dry basis
$\bar{x}$	air specific humidity [kg$_{MC}$·kg$_{d.a}$ $^{-1}$]	*dtf*	dry and tar free basis

(*continued on next column*)

(*continued*)

m	mass [kg]	*gr*	gasification reactor
UC	Unconverted Carbon	*i*	compound in syngas
M	Molar mass	*ogp*	overall gas production
LHV	Lower Heating Value [MJ·Nm^{-3}]	*pb*	power to biomass
$\overline{LHV}$	Lower Heating Value [MJ·kg^{-1}]	*s*	syngas
Y	Yield	*j*	chemical element in biomass
P	Power	$A \rightarrow BA \rightarrow B\dot{m}_{wa\rightarrow m_b}\dot{m}_{wa\rightarrow m_b}$	compound *A* present in system *B*

(*continued on next page*)

This article is part of a special issue entitled: ICCET 2024 published in Energy.

* Corresponding author.
E-mail address: maurizio.grigiante@unitn.it (M. Grigiante).

https://doi.org/10.1016/j.energy.2025.137209
Received 28 March 2025; Received in revised form 1 June 2025; Accepted 18 June 2025
Available online 20 June 2025

(*continued*)

η	Efficiency	*wb*	wet basis
UA	Ultimate analysis	*w*	water
x	Molar fraction of gaseous compounds		
z	Mass fraction of biomass elements		

1. Introduction

Biomass gasification is widely recognized a pivotal technology [1–3] to convert biomass into eco-friendly fuels like syngas and chemical products [4,5]. Syngas generated from gasification is used on power generation technologies as internal combustion engine, gas, steam and micro-gas turbines [6,7], in biomass based combined power cycle [8] and fuel cells [9,10].

Considering the potential and promising expectations placed in these technologies, they are object of study investigated both in the modelling [11–13] and experimental [1,14,15] fields. Biomass, currently available in form of wood chips from forestry activities and wood waste processing [16], is attracting growing interest within renewable energies scenarios [17,18]. Despite this, over the years several peculiarities of raw biomass have been recognized as critical factors capable of influencing the wide diffusion of this resource in the context of energy conversion processes. Those considered particularly critical are: high moisture and oxygen content (approximately 40 %), low energy density (strongly dependent on moisture content (*MC)*), tendency to degrade due to its hydrophilic characteristic, heterogeneous size and shape and low grindability. Furthermore, the complexity of its supply chain management, including harvesting, transport and storage phases, getting worse by the general lack of standardisation procedures, presents many unknowns both in the development of biomass-based energy conversion technologies and in the competitiveness with the traditional energy resources, such as fossil fuels and the other renewable resources. On the other hand, considering its recognized strategic strengths such as its global availability, storage opportunities and on-demand convertibility, this resource can contribute to the constant increase of energy interdependence [18–20] with a limited environmental impact [21]. These expectations, also confirmed by the International Energy Agency [22], recognize in biomass a resource with high potentialities for applications in sustainable technologies, able to contribute for about 10 % of the global energy mix by 2035.

As is known, among the thermal processes, the most common are the direct combustion (the most widespread one) and gasification, followed by carbonization and pyrolysis. Gasification is a thermal process that occurs at high temperatures due to reaction between biomass and one or more gasification agents, usually air, in an oxygen-poor environment to avoid complete combustion. [23,24]. Requiring thermal energy, gasification can therefore be defined as a process that "transfers" energy from the chemical bonds of the biomass constituent fibers (hemicellulose, cellulose, lignin) to the obtained gaseous compound, unlike what happens in combustion which, instead, releases thermal energy. This gives the gasification process the flexible character of a thermochemical process [25] able to treat different types of biomass including low-value lignocellulosic feedstock, waste biomass and, in some cases, waste materials. Furthermore, by controlling the process parameters, it is possible to adjust the composition of the syngas to make it more suitable for specific applications: from heating and power generation [26], including CHP and tri-generation plants [27], from the production of fuel [5] up to high value-added compounds for chemical uses [28,29]. For all these reasons gasification is increasingly recognized a strategic technology to drive the exploitation of biomass resources in years to come [30,31].

However, the use of biomass in gasification processes has encountered specific criticalities related to the complexity of the lignocellulosic matrix itself. This is mainly due to its compactness and to the presence of different bonding forces between the fibres, as the presence of a significant quantity of highly crystalline cellulose molecules [32,33]. In light of these problems, many efforts have been made to study suitable pre-treatments that, in recent years, are acquiring an increasing importance to the point of being considered an essential stage in the enhancement of biomass chain valorization [3]. Pre-treatments, involving thermal, mechanical, physicochemical and biological methods, can have a significant impact on improving both the energy conversion yield of the processes and the quality of the final products. For this reason, the experimental activities presented in this study involve also the gasification of woody biomass previously subjected to torrefaction. This process, classified among the physical-chemical pre--treatments, is carried out in inert atmosphere at temperatures ranging within 200–300 °C, a condition that causes the progressive breakdown of lignocellulosic fibres [34,35]. Jointly with the dehydration of the entire structure, this entails the reduction of O/C and H/C molar ratios. Compared to raw biomass, torrefied wood becomes more hydrophobic and easily grindable, presents a higher *LHV* and greater structural uniformity [36]. This entails a generalized improvement to the characteristics of torrefied biomass compared to raw biomass, as confirmed by several studies [37–39]. The upgrade due to this thermal pre-treatment makes torrefied biomass potentially useable also as partial substitute of solid fuels in different power generation technologies [40,41].

To further increase the competitiveness of biomass utilization, in the last decade, attempts have been made to combining torrefaction with densification. This last pre-treatment, better known for some time as pelletization and now integral part of the biomass supply chain, allows to obtain a stable agglomerate (pellet) starting from raw biomass (chips, slabs, wood work pieces), previously ground, fron the cylindrical shape with a diameter between 6 and 25 mm and length between 3.50 and 50 mm [42,43]. Through this treatment, the density of raw biomass increases from 40 to 200 kg/m^{-3} up to 600–1000 kg/m^{-3} of that in form of pellet, reaching an almost constant *MC* value around 8 %.

The possibility of densifying biomass has contributed to making its logistics chain much more competitive, making the storage, handling and distribution processes much more efficient and fluid-like, thus allowing their final use also through automatic feeding systems (pellet stoves). From an economic point of view, since the value of the biomass supply chain is strongly dependent on the volumetric energy density (MJ/m^3), the increase of this parameter for wood pellet (*WP*), makes its energy cost (€/MJ) more competitive compared to that of forest feedstock. All these aspects have significantly increased the final use of *WP* and the economic value of the biomass [33], classifying, furthermore, this resource as an energy commodity [39].

By combining densification with Torrefaction pre-treatments, higher temperatures are needed but, due to the increased grindability, a lower mechanical energy per unit of biomass treated is reuired. As final result, due to the increased *LHV*, the combination of the two processes leads to a significant increase in the volumetric energy density of torrefied pellet (*TP*) [29]. Considering these, a significant growth is expected also for its use both in energy industries and metallurgical plants in co-firing with coal [44,45]. Looking at the current state of gasification, for several years studies are focused on the following strategic areas: from fundamental to applied research including modelling, to the evaluation of the impact of different biomasses on the process performances up to the economic analysis to assess the role of this process in the emerging energy scenarios. Reference is made to the following papers for an in-depth and up-to-date overview of this technology [1,4,7,19,25,46].

In addition to the intrinsic characteristics of the biomass here outlined, the process is influenced by the type of reactor in which it occurs and by the constraints imposed by the operating conditions. For the purpose some specific parameters have been introduced such as the carbon conversion efficiency (η_{CC}), the cold gasification efficiency (η_C) and the evaluation of tars in syngas. For a wide overview specifically dedicated to detail the role of the parameters of the process, reference is made to the folowing recent publications: Ferreiro et al. [1] and Kuttin

et al. [46].

Regarding the use of torrefied biomass in gasification, while a large number of works has been published on gasification and, separately, on torrefaction, papers dealing with the use of torrefied biomass on gasification are relatively few. Despite this, these studies confirm that torrefaction improves the performances both of the process and of the quality of the syngas [3,14,35,36,47–51]. Furthermore, torrefaction is gaining interest as strategic process to upgrade agricultural waste and residues potentially useable in gasification [52–54]. However, important questions remain open, in particular regarding the comparative analysis of the exercise parameters of the process when fed with raw or, alternatively, with torrefied biomass. Furthermore, by restricting the analysis to the use of TP, the studies and the documented experiences are so far very limited [36,55,56]. The scenarios that emerge from this overview highlight how, both biomass pre-treatments and the knowledge of the impact of the operating conditions, represent the two topics issues on which the research on gasification is mostly oriented. The proposed study fits into this scenario and aims to propose some innovative aspects here highlighted:

- from a methodological point of view, the innovation consists on the design of a batch reactor suitable to be placed on a scale. This solution, allowing the continuous monitoring of the biomass lost ($\dot{m}_{bl}$) during gasification, has suggested the idea of reformulating appropriately the mass and energy balances of the gasifier in order to make them conform to describe those specific of a continuous steady-state gasifier. This approach allows to provide an estimation of the performances of a continuous gasification process by monitoring, for selected air flow rate ($\dot{V}_{a,wb}$) values, only the $\dot{m}_{bl}$ and the char amount (m_{char}) produced from a batch gasifier.
- from an experimental point of view, this work provides a detailed comparisons of the gasification process outcomes, in terms of syngas quality and gasifier performances, when it is powered both with raw and torrefied biomass in form of pellet. This contributes to enlarge the experiments on gasification since limited experiences are documented for *TP* [36,54,55].
- considering the process analysis, this work highlights how, for a selected type of biomass (*WP* or *TP*), the $\dot{V}_{a,wb}$ plays the role of a key parameter of the process through which the trends of the main quantities and those of other parameters can be correlated. In particular, this study highlights the impact of the $\dot{V}_{a,wb}$ on the evolution of both the overall gas production $\dot{m}_{ogp}$ and of the generated m_{char} from which the quality of the obtained syngas, ultimately, depends.

2. Material preparation and characterization

2.1. Material selection

As outlined in the introduction, the emerging perspectives suggest that the strategic use of biomass will inevitably require an articulated supply chain involving thermo-chemical pre-treatments and densification processes [*55*]. These two stages are an integral part of this study since the gassification tests have been carried out using spruce (Picea abies) both as raw and torrefied biomass in form of pellet. Due to the large commercial availability, the EN*plus* A1 certified pellet quality was chosen as reference for *WP*. EN*plus* guarantees the complying with ISO 17225–2:2014 [57] that conforms with the highest quality of graded wood pellet for residential and industrial uses. The same species, spruce feedstock supplied by a local sawmill in the form of wood chips, was first torrefied and then densified to obtain *TP*. The wood, harvested in the fall of 2023 and cut into pieces, was shredded and stored for several months under laboratory conditions. Thereafter this shredded material was sieved to separate it into different sizes. Specimens larger than 4 mm but less than 12 mm were selected before proceeding with their characterization, torrefaction and pelletizing treatments.

2.2. Torrefaction

A bench torrefaction pilot plant was specifically assembled to prepare the torrefied material for this gasification campaign. The torrefaction reactor has been built according to a previous reactor design whose description is detailed in the Authors' publication [58]. To increase the production of the torrefied material the new bench scale reactor has been enlarged to 1500 mm in length and 60 mm in diameter. This allows to treat an amount of about 300 g of the selected woodchips with respect to the limited capacity of 45 g of the previous plant. Before torrefaction, the woodchips were dried at 105 °C for several hours and their *MC* determined in triplicate according to AOAC standard method 930.15 [59]. A direct heating approach has been adopted integrated also with electrical heaters positioned all around the external surface of the reactor to achieve a better control of the torrefaction temperature to avoid, in particular, overshoot conditions. This control has been intensified with further thermocouples regularly positioned inside and around the external surface of the reactor as well as at the inlet section of the reactor to monitor the temperature of nitrogen used as heating carrier. This has allowed to pursue a high homogeneity degree for the resulting torrefied material and to test the very satisfactory reproducibility of the experimental runs required to achieve the final amount of 10 kg of torrefied biomass. The woodchips charge has been maintained for 50 min at a selected torrefaction temperature of 290 °C. The resulting mass yield can be referred to a target value close to 80 %. Further details of the process can be found on the cited paper [58]. The material obtained after each torrefaction run has been collected into sealed bags, mixed and milled by a *Cutting Mill Pulverisette 19* (Fritsch, Germany) to provide a final fineness of the particles below 0.5 mm. Before pelletizing, the grinded material was re-wetted with a sprayer and mixed inside a plastic storage container to achieve a homogeneous MC_{db} (dry basis) nearby 30 %. Successively, to maintain this condition, the material was placed into sealed bags for 48 h and transferred to a conditioned room with a constant temperature of 27 °C.

2.3. Densification

Densification of the torrefied material was performed through pelletization by using a pellet mill flat ring die *Model PLT-100* (Smartec, Italy). This machine is characterized by the fact that the die, through which the raw material is forced, is flat like a plate. It is usually turned by a set of gears called "*ring and pinion gear*". In this model, widely diffuse, the material is force by two electrically driven rollers while the die is stationary. The die has a diameter of 12 cm and a thickness of 3,8 cm. It presents approximately one hundred holes of 6 mm diameter drilled in the die so that the formed pellets are approximately 6 mm in diameter and 18 mm in length. According to manufacturer's specifications, this model has a productivity ranging from 40 to 70 kg/h. To determine the dimensions and unit mass of the obtained *TP*, they were randomly selected before each gasification run. Using a digital vernier caliper with a 10^{-2} resolution, the following value for length (L) and diameter (D) were measured: L = 18,42 ± 0,40 mm; D = 6,04 ± 0,002 mm. The mass of each TP was determined with a digital balance (10^{-4} g resolution). From these measurements the density of TP pellet and, similarly, of *WP has been estimated:* $\rho_{TP} = 1{,}21 \pm 0{,}009$ (g/cm^3) and *WP* $\rho_{WP} = 1{,}14 + 0{,}005$(g/cm^3).

2.4. Material characterization

Ultimate Analysis (*UA*) including ash content and Lower Heating Value (*LHV*) have been determined for both *WP* and *TP*. Carbon, hydrogen, nitrogen and sulphur (CHNS) content was measured by using the Elemental Analyzer Mod. Vario Macro Cube-Elementar (Elementar Analysen Systeme GmbH, Hanau, D) while the oxygen content was

calculated by difference from the total. The ash content was determined according to the standard method DD CEN/TS 14775:2004 [60] while the *LHV* was measured by the Oxigen Bomb Calorimeter Mod. IKA C5000 (Isoperibolic Calorimeter). All these anaes have been performed by triplicate and the resulting average values reported in Table 1. The *MC* percentage (%), on a wet basis (MC_{wb}), has been measured for each sample before starting each gasification test, according to the cited method [60], and the values included in Table 3 of section 3.3.

3. Gasification pilot-plant

3.1. Description of the updraft fix bed gasifier

A laboratory-scale batch micro-gasifier has been specially developed for this investigation. The reactor consists of a cylindrical vessel of stainless steel of 60 mm in diameter and 1300 mm in length and operates at atmospheric condition. Before each test, an amount of about 2 kg of pellets is fully loaded from the top of the reactor. The material is propped up by a grid placed at a distance of 100 mm from the bottom of the reactor. By means of a controlled compressed air line, the air flow rate, used as gasification agent (primary air), enters the reactor at the bottom through a hole drilled in the centre of the base of the reactor. Making reference both to the air (bottom entry) and syngas (top exit) flow rates, this reactor looks like an updraft fixed-bed gasifier [61]. On the other side, since the biomass is not fed according to a continuous flow configuration, the reactor could also be traced back to a fixed bed batch type. It should be noted that the biomass bed does not move except for the shrinkage of volume caused by the process itself. In fixed-bed gasifiers, the gasification process occurs in several stages, each one taking place in specific sections of the biomass bed. The configuration of the bed sections depends on the type of gasifier (updraft, downdraft, cross-draft) that, in turn, affects the quality of the obtained syngas. The configuration of the stages that characterizes this gasifier is represented in the diagram of Fig. (1) and refers to a generic working condition which, as explained in the next paragraph, can be traced back to a steady state working condition. After loading the reactor, an excess air flow rate is initially introduced into the reactor to promote the combustion process by igniting the biomass bed from above. In a very short time the air flow is reduced to bring the combustion back to a sub-stoichiometric condition to oxidize the biomass only partially. The air (gasification agent), which flows upwards through the biomass, feeds the combustion zone whose front moves, therefore, from the top to the bottom through the unburned biomass bed (*stage* 1). The combustion reactions raise the temperature around this area which, as detected by the monitoring carried out during the tests, settles at a maximum value close to 1000 °C. In the scheme this stage is identified as oxidation, *stage 2*. This condition activates the pyrolysis process (*stage 3*), a thermochemical breakdown that converts the biomass components into: a volatile fraction, light hydrocarbons, CO, CO_2 and *tars*, a condensable fraction that develops at low temperature in oxygen-free zones with the temperature ranging from 200 to 450 °C; a solid fraction, named *char*, whose layer constitutes the reduction zone, usually named *gasification stage* and indicated as *stage 4* in Fig. (1).

This section of the biomass bed represents the core of the gasification process since the flow of the gaseous compounds, generated in the

Table 1
UA including ash % and *LHV* for *WP* and *TP*.

Sample*	C [wt. %]	H [wt. %]	N [wt. %]	S [wt. %]	O [wt. %][a]	Ash [wt. %]	*LHV* [MJ/kg]
WP	50,22	6,12	0,01	0,11	43,22	0,32	17,21
TP	53,77	5,98	0,11	0,01	39,03	1,10	19,67

* All values are expressed as mass fraction on a dry basis.
[a] Oxygen fraction calculated by difference.

Table 2
Sequence of stages and corresponding reactions for the proposed gasifier scheme (Fig. 1). ΔH values are referred to standard conditions [29].

stage	type of stage	reactions			
1	*Unburned biomass*	–			
2	*Oxidation*	Heterogeneous Reactions			
		Complete oxidation:	$C + O_2 \rightarrow CO_2$:	ΔH = -393.7 kJ/mol	[29,65,66]
		Partial oxidation:	$C+0.5\ O_2 \rightarrow$ CO:	ΔH = −119.6 “	
		Homogeneous Reactions			
		Water gas shift reaction: (WGS)	$CO + H_2O \leftrightarrow CO_2 + H_2$:	ΔH = -41.2	
			$H_2 + 0.5\ O_2 \leftrightarrow H_2O$:	ΔH = -241.1	
			$CO + 0.5\ O_2 \leftrightarrow CO_2$:	ΔH = -283.0	
		Methanation reactions:	$2CO + 2H_2 \leftrightarrow CH_4 + CO_2$:	ΔH = -247.3	
			$CO + 3H_2 \leftrightarrow CH_4 + H_2O$:	ΔH = -206.2	
		Methane ref. reactions:	$CH_4 + 1.5\ O_2 \leftrightarrow CO + 2H_2O$	ΔH = -36.2	
			$CH_4 + H_2O \leftrightarrow CO + 3H_2$	ΔH = +206.2	
3	*Pyrolysis*	Biomass → heavy and light species + gases + H_2O + tars + char ΔH> 0			[67–69]
4	*Gasification (reduction)*	Boudouard reaction:	$C + CO_2 \leftrightarrow 2CO$;	ΔH = +175.52	[70–72]
		Carbon steam reforming:	$C + H_2O \leftrightarrow CO + H_2$	ΔH = +131.20	
		Hydrogasific. reaction:	$C + 2H_2 \leftrightarrow CH_4$	ΔH = -74.87	
		Tar reforming:	tars + $H_2O \rightarrow CO + H_2$	ΔH > 0	
		Tar cracking:	tars + $O_2 \rightarrow CO + H_2O$	ΔH > 0	
			tars + $CO \rightarrow CO_2 + H_2 + CH_4$	ΔH > 0	
5	*No reactive char*	–			

Table 3
Biomass charge and corresponding *MC* % values. $\dot{V}_{a,wb.}$ values and monitored $\dot{m}_{bl}$ results for *WP* and *TP* tests. Solid symbols ●, ■, ▲: tests carried out at the same $\dot{V}_{a,wb}$.

	Biomass specification		*Basic process quantities*	
Tests	m_b (*charge*) [kg]	MC_{wb} [% wt.]	$\dot{V}_{a,wb}$ ($\dot{m}_{a,wb}$) [Nl·min^{-1}] (kg·h^{-1})	$\dot{m}_{bl}$ [kg·h^{-1}]
WP-1●	1.90	6.92	15(1.10)	0.63
WP-2	1.85	6.48	17(1.25)	0.67
WP-3■	1.85	7.00	19(1.40)	0.71
WP-4	1.85	6.99	21(1.54)	0.74
WP-5▲	1.85	6.87	23(1.69)	0.78
WP-6	1.85	6.56	25(1.84)	0.80
TP-1●	1.80	3.90	15(1.10)	0.66
TP-2■	1.80	3.85	19(1.40)	0.74
TP-3▲	1.85	3.89	23(1.69)	0.84
TP-4	1.78	5.59	27(1.98)	0.89
TP-5	1.75	5.62	30(2.20)	0.93

* wet basis.

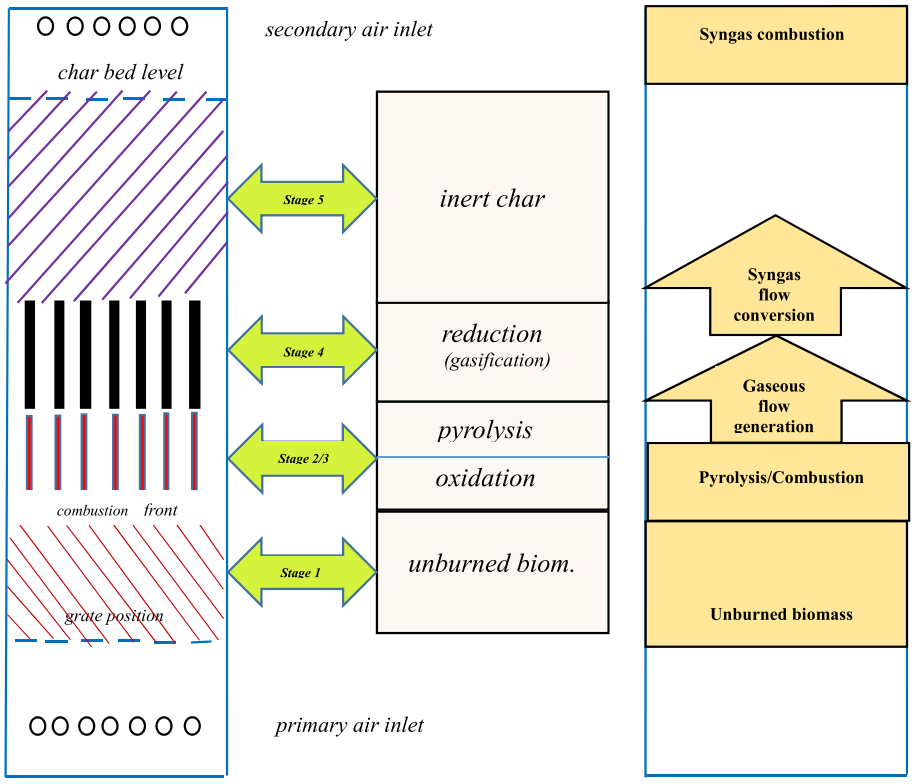

Fig. 1. Scheme of the reactor stages in correspondence to a generic time-set.

underlying stages and flowing upwards, in contact with the high temperatures of this char layer, undergo endothermic reduction reactions that convert it into syngas, the final product of the gasification process. Furthermore, in this stage, the radicals released during oxidation can react both in gas phase to reform the tar species and with the solid matrix to release further combustible gases [50,62–65].

The heat absorbed by the endothermic reactions progressively reduces the temperature of the char layer as one moves upwards, giving rise to the inert zone indicated as *stage* 5 (Fig. 1). For sake of clarity, it is to point out that the proposed description and the corresponding scheme of Fig.(1) provide a useful but simplified schematization of the complexity of the process under consideration.

In particular, it should be considered that the identified phases are never perfectly separated from each other as emerges from the proposed description but overlapped. This condition, in particular, involves the combustion and pyrolysis stages. It follows that the attribution of specific reactions to each single phase reported in Table 2 must be considered in the context of a simplified schematization to help the comprehension of the different steps of the process.

3.2. Description of the overall pilot-plant

The novelty of this work consists in the continuous monitoring of the m_{bl} during the entire gasification process by positioning the reactor on a suitable scale. A laboratory Helmac digital scale, Mod. ASW30, has been utilized. This scale has a maximum weighing capacity of 30 kg and an accuracy of three digits after the decimal point (0.001 kg). The experimental quantities has been monitored by equipping the pilot plant with suitable instrumentation. The primary air flow rate ($\dot{V}_{a,wb}$) to the gasifier is supplied from an air compressor and is measured by a variable air flow meter (Bronkhorst, Mod. F-201AB) covering the range from 0,4 to 70 Nl·min^{-1} (accuracy 1 %). Temperatures are monitored by four *k type* thermocouples with a measurement range from −10 °C to 1000 °C (uncertainty ± 0,75 %), connected to a data logger acquisition device (Agilent 34972A LXI). They are positioned inside the biomass bed along the axis of the reactor and equally spaced at a distance of 10 cm. The entire external surface of the reactor is insulated by a continuous ceramic wool swab. A sampling line, located at the upper part of the char section, sucks an appropriate syngas flow whose composition is detected and recorded on line by electrochemical sensors equipped on a syngas monitor device (MRU GmbH Delta 1600). Prior to analysis, the syngas sample flows through a cleaning section consisting of three small containers (bottles) located upstream of the syngas analyser and acting as a trapping device for condensable compounds (*water* and *tars*). In addition, to protect the MRU device, the clean syngas, before being inserted into the analyser, is passed through a final filter to remove carbon soot particles. The indicated instruments and connections have been equipped to avoid interferences with the biomass loss monitoring. The following Figs. (2a, 2b) depict the results of the on-line monitoring both of the biomass loss (2a) and of the molar fraction percentage (%) (2b) of

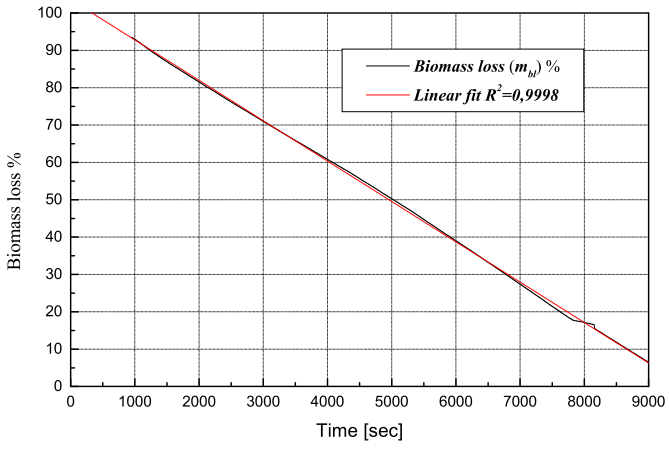

Fig. 2a. Trend of the biomass loss for a complete gasification test including the R^2 parameter of the linear regression.

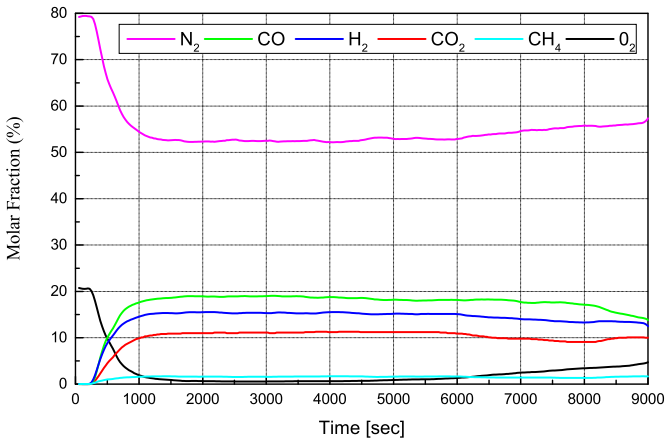

Fig. 2b. Trends of the mole fractions of the syngas components for a complete gasification test.

the syngas components referred to the overall time frame of a generic test. This clearly shows how these quantities maintain a nearly constant trend throughout the entire process. As proposed below, this behaviour has allowed to elaborate an innovative procedure to express the mass and energy balances of the gasifier conforming to those pertaining to a continuous steady-state updraft fixed-bed configuration. Among studies involving both batch and continuous gasifier, significant experimental research activities have investigated the comparison of the two configurations [73–75] Others studies have compared the performances between steady-state and transient conditions imposed to batch gasifier [76,77]. To Authors' knowledge, a significant research work that introduces an experimental approach similar to that followed in this work is that proposed by Carmona et al. [78] in which, in particular, the mass loss is measured by placing the reactor on a load cell.

3.3. Experimental planning

Six tests have been carried out for *WP,* named from *WP-1* to *WP-6,* and five for *TP* named from *TP-1* to *TP-5*. The following Table 3 reports the $\dot{V}_{a,wb}$ used for each test: starting from 15 to 25 Nl·min^{-1} with regular increments of 2 Nl·min^{-1} for *WP*; starting from 15 to 30 Nl·min^{-1} with regular increments of 3 Nl·min^{-1} for *TP*. To better understand the reason of this choices, reference is made to paragraph 5, *Results and Discussion*. The number in brackets indicates the air mass flow rate on a wet basis ($\dot{m}_{a,wb}$) expressed as kg·h^{-1}. This has been obtained by converting the $\dot{V}_{a,wb}$ through the wet air density value: $\rho_{a,wb}$ = 1,224 kg m^{-3} in turn referred to the specific humidity value of air: $\bar{x}$ = 0.01 $kg_{MC}/kg_{a,db}$ corresponding to the average environment conditions of the laboratory during the tests. As far as possible we tried to charge the reactor with the same amount of biomass (≈1,75-1,90 Kg). A Helmac digital scale, Mod. ASW3 (maximum weighing capacity 3 kg, accuracy 0.001 kg) has been used to weigh the biomass to be treated. These data are reported in Table 3 with their corresponding MC_{wb} measured before starting each test. This Table includes also the biomass loss flow rate ($\dot{m}_{bl}$) obtained from the elaboration of the data trends as that depicted in previous Fig. (2a). To make reading the data simpler and more immediate, in all the Tables the values are approximated to two digits after the decimal point. Regarding the analysis of the experimental measurements, reference is made to paragraph 6 dedicated to their statistical analysis.

4. Proposed procedure

4.1. Mass balance

4.1.1. Overall mass balance

Making reference to the resulting steady state condition of the process, the overall gas mass flow rate production of gas ($\dot{m}_{ogp}$) can be expressed as sum of the $\dot{m}_{bl}$ and $\dot{m}_{a,wb}$ quantities whose values are reported in the previous Table 3:

$$\dot{m}_{ogp} = \dot{m}_{bl} + \dot{m}_{a,wb} \tag{1}$$

As detailed in the following Eq. (5), the term $\dot{m}_{ogp}$ includes the *MC* $\dot{m}_{w\to ogp}$ and the *tars* $\dot{m}_{tars\to ogp}$ mass flow rates in the produced gas. Since the amount of char (m_{char}) present inside the reactor at the end of each test has been rigorously weighed, also the produced char can be expressed in terms of *char* mass flow rate ($\dot{m}_{char}$) considering the following reasonable assumption:

- the ratio between the char flow rate and the biomass lost flow rate $\dot{m}_{char}/\dot{m}_{bl}$ can be assumed equal to the ratio between the quantity of *char* produced and the treated biomass charge,

m_{char}/m_b, so obtaining the $\dot{m}_{char}$ as:

$$\dot{m}_{char} = \frac{m_{char}}{m_b}\cdot\dot{m}_{bl} \tag{2}$$

Thus estimated the $\dot{m}_{char}$ and $\dot{m}_{bl}$ quantities, also the amount of biomass treated in the batch reactor can be expressed in terms of biomass flow rate ($\dot{m}_b$) feeding a continuous steady-state updraft fixed-bed gasifier:

$$\dot{m}_b = \dot{m}_{bl} + \dot{m}_{char} \tag{3}$$

Rearranging Eqs. (1) and (3), the resulting Eq. (4):

$$\dot{m}_b + \dot{m}_{a,wb} = \dot{m}_{ogp} + \dot{m}_{char} \tag{4}$$

corresponds to the one that would be obtained by applying the mass balance to a continuous steady state reactor configuration. Fig. (3) shows a scheme of the gasification plant. All quantities are expressed in terms of mass flows including, in brackets, the quantities converted to "*virtual*" mass flow rates by applying the proposed approach.

For each test, the following Table 4 reports the results of the elaborations including the measured m_{ch}/m_b ratio (% wt).

Eq. (4) can be rearranged into a more detailed form to highlight the contributions of the individual quantities in the overall mass balance. The term $\dot{m}_b$ can be split into two contributions: one to account for the dry biomass ($\dot{m}_{b,db}$), the other for the *MC* in biomass ($\dot{m}_{w\to b}$).

The same can be done for the term $\dot{m}_{a,wb}$, splitting it into the dry air

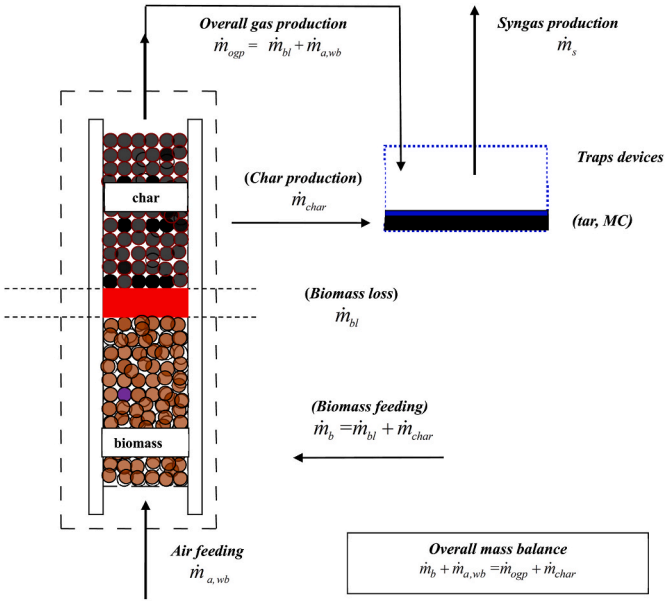

Fig. 3. Scheme of the overall gasification plant.

Table 4
Results of the quantities in terms of mass flow rate [kg·h^{-1}] as results of the proposed procedure.

Tests[a]		$\dot{m}_{ogp}$ [kg·h^{-1}]	m_{char}/ m_b [% wt.]	$\dot{m}_{char}$ [kg·h^{-1}]	$\dot{m}_b$ [kg·h^{-1}]
WP-1●	(15)	1.73	9.17	0.058	0.690
WP-2	(17)	1.92	8.38	0.056	0.728
WP-3■	(19)	2.10	6.34	0.045	0.751
WP-4	(21)	2.29	3.31	0.025	0.769
WP-5▲	(23)	2.47	1.21	0.009	0.790
WP-6	(25)	2.65	0.50	0.004	0.810
TP-1●	(15)	1.76	19.81	0.131	0.791
TP-2■	(19)	2.14	16.52	0.123	0.868
TP-3▲	(23)	2.53	10.05	0.085	0.927
TP-4	(27)	2.87	5.81	0.052	0.942
TP-5	(30)	3.13	2.10	0.019	0.952

[a] In brackets the air flow rate $\dot{V}_{a,wb}$ (Nl·min^{-1}); symbols ●, ■, ▲: tests carried out at the same $\dot{V}_{a,wb}$.

contribution ($\dot{m}_{b,db}$) and that pertaining to the *MC*, $\dot{m}_{w\to a}$. Analogously, the quantity $\dot{m}_{ogp}$ can be expressed as sum of three contributions: the first accounts for the final syngas amount $\dot{m}_s$. In this analysis this quantity is determined by expressing the $\dot{m}_{ogp}$ on a dry and tar free basis: $\dot{m}_s = \dot{m}_{ogp,dtf}$; the second accounts for its *MC*, $\dot{m}_{w\to ogp}$; the third for the *tars*, $\dot{m}_{tars\to ogp}$. The $\dot{m}_{char}$ can likewise be subdivided into the *ash* and the unconverted carbon (*UC*) flow rates contributions, $\dot{m}_{ash\to char}$ and $\dot{m}_{UC\to char}$ respectively.

Eq. (4) can then be rewritten into the following explicit Eq. (5):

$$\dot{m}_{b,db} + \dot{m}_{w\to b} + \dot{m}_{a,db} + \dot{m}_{w\to a} = \dot{m}_s + \dot{m}_{w\to ogp} + \dot{m}_{tars\to ogp} + \dot{m}_{ash\to char} + \dot{m}_{UC\to char} \quad (5)$$

4.1.2. Elementary mass balance

Eq. (5) facilitates the elaboration of both the elementary mass balance and the determination of some specific parameters of the process. In particular, it allows to utilise directly the data of the syngas composition which, as described in Section 3.2, is detected on a dry and tar-free basis. It is important to observe that, in addition to the gaseous compounds, moisture and *tars*, the $\dot{m}_{ogp}$ quantity includes also traces of minor C_xH_y compounds, HCl, HCN, NH_3, metals and alkali components. Sulphur is converted mainly into H_2S, then into Carbonyl Sulphide (COS) that, interacting with O_2, leads to SO_2 [79]. Some sulphur compounds can be found into ashes but their concentration, as reported by Kaewluan et al. [80], are normally around few ppm. Since the amounts of these species are extremely small, they have not been taken into account in the continuation of this elaboration.

As proposed in the following Eq. (6), Eq. (5) can be further rewritten by including the chemical elements of the biomass and of the gaseous species of the syngas:

$$\dot{m}_{b,db}(z_C + z_H + z_O + z_N + z_{ash}) + \dot{m}_{a,db} + \dot{m}_{w\to b} = \dot{m}_s \cdot \left(\sum_i x_i \cdot \frac{M_i}{M_s}\right) + \dot{m}_{w\to ogp} + \dot{m}_{tars\to ogp} + \dot{m}_{ash\to char} + \dot{m}_{UC\to char} \quad (6)$$

The z_j term indicates the mass fraction of each of the chemical elements (*j*=*C,H,O,N, ash*) of the biomass whose values are reported in Table 1. The MRU device provides the composition of the syngas, expressed in terms of molar fraction x_i (*dtf basis*), for each of the *i*th compound (*i* = *CO, CO_2, CH_4, H_2, N_2*) of the $\dot{m}_s$. To keep Eq. (6) consistent, the syngas composition is converted into the mass fraction knowing the molar mass of each species (M_i) and that of the syngas (M_s).

- *Nitrogen mass balance:*

Following the widely adopted assumption [29] that, in gasification processes involving biomass, nitrogen can be considered as an inert gas, the steady state equation of the mass balance of nitrogen ($N_{2\ input} = N_{2\ output}$) can be solved with respect to the unknown $\dot{m}_s$ term:

$$\dot{m}_{a,db} \cdot y_{N_2} + \dot{m}_{b,db} \cdot z_N = \dot{m}_s \cdot x_{N_2} \cdot \frac{M_{N_2}}{M_s} \quad (7)$$

where y_{N_2} is the mass fraction of N_2 in air. This quantity allows to calculate a parameter considered significant for the performance of the gasification process: the *syngas yield* (Y_s), defined as the ratio of the volumetric syngas production $\dot{V}_s$ ($Nm^3 \cdot h^{-1}$) to the biomass flow rate feeding the reactor:

$$Y_s = \frac{\dot{V}_s}{\dot{m}_b} \quad (8)$$

The $\dot{V}_s$ has been obtained by converting the $\dot{m}_s$ using the M_s and, as molar volume, the value equal to 22.414 Nm^3/kmol assuming the syngas as ideal gas at normal temperature and pressure conditions (NTP). These data are reported in the following Table 5.

- Hydrogen mass balance.

The following Eq. (9a) takes into account the total inflow of hydrogen into the gasifier due to biomass, the moisture in biomass and in the air:

$$\dot{m}_{H_{2,input}} = \dot{m}_{b,db} \cdot z_H + \left(\dot{m}_{w\to b} + \dot{m}_{a,db} \cdot \bar{x}\right) \Big/ 9 \quad (9a)$$

where $\bar{x}$ indicates the specific humidity of air.

Eq. (9b) accounts the hydrogen leaving the gasifier as H_2 and CH_4:

$$\dot{m}_{H_{2,output}} = \left(x_{H_2} + 2 \cdot x_{CH_4}\right) \cdot 2 \,/\, M_s \cdot \dot{m}_s \quad (9b)$$

According to Basu [29], the *MC* in the $\dot{m}_{ogp}$ is associated with the hydrogen balance between the inlet and outlet flow from the reactor and is therefore determined as:

$$\dot{m}_{w\to ogp} = \left(\dot{m}_{H_{2,input}} - \dot{m}_{H_{2,output}}\right) \cdot 18 \,/\, 2 \quad (10)$$

Considering the three contributions of the overall produced gas introduced into Eq. (5), once the syngas $\dot{m}_s$ and moisture $\dot{m}_{w\to ogp}$ have been determined, Eqs. 7 and 10, the *tars* flow rate ($\dot{m}_{tars,db}$) can be estimated as:

$$\dot{m}_{tars,db} = \dot{m}_{ogp} - \dot{m}_s - \dot{m}_{w\to ogp} \quad (11)$$

- Carbon mass balance:

Rigorously, the carbon (C) mass balance cannot be performed since the *UA* for *tars* and *char* has not been carried out. However, the carbon conversion efficiency, η_{CC}, defined as the ratio between the C content in syngas to that in the loaded biomass:

$$\eta_{CC} = \frac{\dot{m}_{C\to s}}{\dot{m}_{C\to b}} \quad (12)$$

can be calculated by the following two equations:

$$\dot{m}_{C\to b} = \dot{m}_{b,db} \cdot z_C \quad (13)$$

$$\dot{m}_{C\to s} = \left(x_{CO} + x_{CO_2} + x_{CH_4}\right) \cdot M_c \cdot \frac{\dot{m}_s}{M_s} \quad (14)$$

The results of these elaborations are reported on the following Table 5. Following the conventional indications, the *MC* in syngas ($\dot{m}_{w\to ogp}$) is here expressed as specific humidity $\bar{x}_s$, defined as the ratio between the quantities $\dot{m}_{w\to ogp}$ and $\dot{m}_s$. Besides the generated $\dot{m}_{tars\to ogp}$, Table 5 includes also the concentration of *tars*, expressed as ratio

Table 5
Results of the quantities obtained from the elementary and mass balance.

Tests[a]	$\dot{m}_s$ (M_s) [kg·h^{-1}]	$\dot{V}_s$ [Nm^3·h^{-1}]	Y_s [Nm^3·kg^{-1}]	$\bar{x}_s$	$\dot{m}_{tars\rightarrow ogp}$ [kg·h^{-1}]	$\dot{m}_{tars\rightarrow ogp}$/ $\dot{V}_s$ [kg·Nm^{-3}]	η_{CC}
WP-1 ●	1.44 (26.40)	1.22	1.77	0.16	0.064	0.052	0.64
WP-2	1.63 (26.22)	1.39	1.91	0.14	0.061	0.044	0.69
WP-3 ■	1.81 (26.10)	1.56	2.07	0.12	0.065	0.042	0.75
WP-4	1.99 (25.98)	1.71	2.23	0.11	0.079	0.046	0.81
WP-5 ▲	2.15 (25.61)	1.88	2.38	0.10	0.095	0.050	0.84
WP-6	2.27 (26.46)	1.93	2.38	0.11	0.110	0.057	0.83
TP-1 ●	1.48 (25.67)	1.29	1.63	0.16	0.057	0.044	0.54
TP-2 ■	1.86 (25.59)	1.62	1.87	0.12	0.061	0.038	0.62
TP-3 ▲	2.22 (25.44)	1.96	2.11	0.10	0.095	0.049	0.70
TP-4	2.55 (25.41)	2.25	2.39	0.09	0.101	0.045	0.80
TP-5	2.80 (25.54)	2.46	2.58	0.08	0.108	0.044	0.87

[a] Solid symbols ●, ■, ▲: tests carried out at the same $\dot{V}_{wet\ air}$.

between the generated *tars* with respect to the $Nm^3{\cdot}h^{-1}$ of syngas produced.

4.2. Energy quantities

The syngas *Lower Heating Value* (LHV_s), expressed in MJ·Nm^{-3}, is determined according to the following equation [29]:

$$LHV_S = 12,696{\cdot}x_{co} + 10,769{\cdot}x_{H_2} + 35,866{\cdot}x_{CH_4} \quad (15)$$

The *Power* of the *gasification reactor* (P_{gr}), alternatively named *potential energy output*, is determined by the product of the $\dot{m}_s$ by the corresponding $\overline{LHV}_s$, obtained by converted the quantity LHV_s into MJ·kg^{-1} by assuming, as *normal molar density* of the syngas (ideal gas), the value: 0,0466 kmol·Nm^{-3}:

$$P_{gr} = \dot{m}_s{\cdot}\overline{LHV}_s \quad (16)$$

Another parameter indicative of the gasification performance is the *Power to biomass yield* (Y_{pb}), defined as the ration between the P_{gr} and the feeding biomass flow rate ($\dot{m}_b$):

$$Y_{pb} = \frac{P_{gr}}{\dot{m}_b} \quad (17)$$

Among the various options used to define the efficiency of the gasification process, the *cold gasification efficiency* η_C is, usually, the most utilized due to low temperatures (ambient condition) reached by the syngas during cleaning processes. The η_C is defined as the ratio of the P_{gr} to that of the feeding biomass excluding, so that, the sensible heat contribution of the syngas at the gasifier output conditions:

$$\eta_C = \frac{P_{gr}}{\dot{m}_b{\cdot}LHV_b} \quad (18)$$

The values of these parameters and the x_i of the compounds involved in *LHV* calculation are reported for each test in the following Table 6.

5. Results and discussion

First of all, it is important to underline that the maximum values of $\dot{V}_{a,wb}$ have been fixed equal to 25 Nl·min^{-1} and 30 Nl·min^{-1}for *WP* and *TP* respectively. These limits are due to the presence of a fluid-dynamic drag/fluidization regime that is triggered following the increase of the air speed for $\dot{V}_{a,wb}$ beyond the indicated limits. This quantity is of primary importance, not only because the dynamic regime of the fluid that is established depends primarily on the $\dot{V}_{a,wb}$ values but, as in this work, air constitutes the gasification agent of the process. The basic idea that guided this experimental work was, primarily, to assess the role of the $\dot{V}_{a,wb}$ on the performances of the process and, furthermore, to evaluate the impact that biomasses, presenting different structures as *WP* and *TP,* have on these. For this reason, in almost all the diagrams shown below,

Table 6
Molar fractions of compounds involved in *LHV* calculation and Energy parameters results.

Tests	x_{co} [%]	x_{H_2} [%]	x_{CH_4} [%]	LHV_s [MJ·Nm^{-3}]	P_{gr} [kW]	Y_{pb} [Kw/(kg$_b$·h^{-1}]	η_C
WP-1	15.46	13.9	2.31	4.28	1.45	2.10	0.47
WP-2	16.10	14.4	2.08	4.33	1.68	2.30	0.51
WP-3	16.75	14.58	1.85	4.35	1.88	2.50	0.56
WP-4	17.89	14.53	1.58	4.39	2.10	2.72	0.61
WP-5	18.37	14.08	1.35	4.32	2.26	2.86	0.64
WP-6	18.10	12.29	1.31	4.08	2.18	2.70	0.60
TP-1	15.40	16.57	2.57	4.66	1.66	2.10	0.39
TP-2	16.73	16.32	2.37	4.72	2.13	2.46	0.46
TP-3	18.51	16.08	2.08	4.82	2.62	2.82	0.54
TP-4	20.58	15.37	1.48	4.78	3.00	3.18	0.61
TP-5	21.59	14.50	1.22	4.73	3.23	3.40	0.66

the $\dot{V}_{a,wb}$ is assumed as independent variable.

The order followed for the presentation of the Figures aims to highlight, in particular, the following:

- to compare, for the two biomasses, the trends of the quantities resulting from the proposed procedure;
- to assess the impact of the progressive reduction of char amount on the quality of the produced syngas and on the performances of the gasifier.

For sake of clearness, it was deemed more appropriate to present first the results related to mass balance (section 5.1) and, subsequently, those related to energy balances (section 5.2).

5.1. Mass balances results

The following Fig. (4) provides a preliminary overview, both for *WP* and *TP*, of $\dot{m}_{ogp}$, $\dot{m}_s$ and $\dot{m}_{bl}$ trends Vs. $\dot{V}_{a,wb}$. First of all it is found that these quantities presents almost overlapping profiles for both biomasses, with a slight increasing difference as $\dot{V}_{a,wb}$ increases. Considering tests of Tables 3–5 presenting the same $\dot{V}_{a,wb}$ (values equal to 15, 19 and 23 Nl·min^{-1}), the maximum percentage difference between *WP* and *TP* stands at 7.8 %. This outcome indicates that torrefaction has a moderate

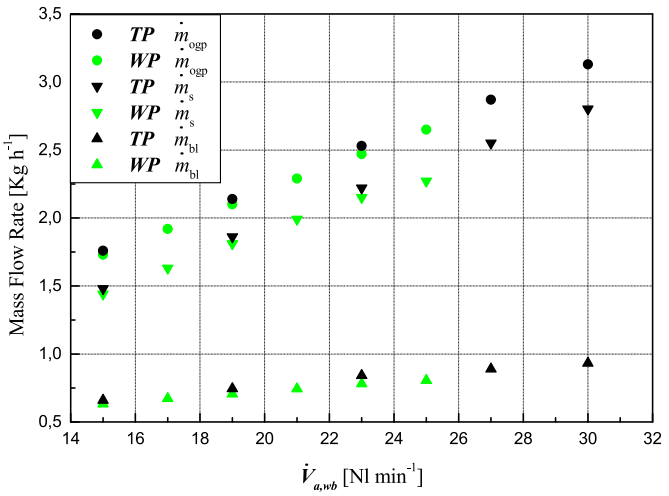

Fig. 4. $\dot{m}_{ogp}$, $\dot{m}_s$ and $\dot{m}_{bl}$ for *TP* and *WP* Vs. the selected $\dot{V}_{a,wb}$ values.

impact on these quantities.

For $\dot{m}_b$, the difference (%) between *TP* and *WP* is more relevant as $\dot{V}_{a,wb}$ increases, moving from 14.64 % to 17.34 % for 15 Nl·min^{-1} to 23 Nl·min^{-1} respectively (Table 4). Considering the mass balance defined by Eq. (3) and the small difference between *TP* and *WP* for the $\dot{m}_{bl}$ (Fig. 4), the increasing difference of $\dot{m}_b$ between *TP* and *WP* is substantially attributable to $\dot{m}_{char}$ as evidenced in following Fig. (5).

Further interesting observations can be drawn by analysing in details the trend of the generated $\dot{m}_{char}$:

- taking into account the very weak dependence of the quantity $\dot{m}_{ogp}$ from the type of biomass (Fig. 4), for tests carried out at the same $\dot{V}_{a,wb}$ the global mass balance, Eq. (4): $\dot{m}_b + \dot{m}_{a,wb} = \dot{m}_{ogp} + \dot{m}_{char}$ can be rewritten as follows:

$$(\dot{m}_b)_{TP} - (\dot{m}_b)_{WP} \approx (\dot{m}_{char})_{TP} - (\dot{m}_{char})_{WP} \quad (19)$$

where the symbol ≈ accounts for the limited discrepancies of $\dot{m}_{ogp}$ for *TP* and *WP*. This is evidence also in Fig. (5) in correspondence of the three common values of $\dot{V}_{a,wb}$.

- Fig. (5) highlights that, for *WP*, the $\dot{m}_{char}$ practically disappears at the higher acceptable values of $\dot{V}_{a,wb}$ (from Table 4: $\dot{m}_{char}$ = 0,009–0,004 kg h^{-1} for $\dot{V}_{a,wb}$ = 23–25 Nl·min^{-1}) while, for *TP*, the $\dot{m}_{char}$ presents an order of magnitude higher also at higher $\dot{V}_{a,wb}$ values ($\dot{m}_{char}$ = 0,052–0,019 kg h^{-1} for $\dot{V}_{a,wb}$ = 27–30 Nl·min^{-1}). As a direct consequence of the observed $\dot{m}_{char}$ trends, the evolution of the $\dot{m}_{bl}$ and $\dot{m}_{b.}$ quantities present the trends depicted in Figs. (6a, 6b). For clarity of the representation, two separate diagrams have been provided for the two biomasses: Fig. (6a) for *WP*, Fig. (6b) for *TP*.

For *WP*, these diagrams show how, as the $\dot{V}_{a,wb}$ increases, the difference between $\dot{m}_b$ and $\dot{m}_{bl}$ decreases rapidly (Fig. (6a)). Correspondently, the $\dot{m}_{char}$ values are almost equal to zero already for $\dot{V}_{a,wb}$ close to 21 Nl·min^{-1}, a condition that involves equality of the two quantities $\dot{m}_b$ and $\dot{m}_{bl}$. This is an indirect proof of the fact that, as the $\dot{V}_{a,wb}$ increases, the gasification stage evolves towards a regime gradually dominated by combustion. As this condition prevails, a progressive reduction of the char layer is observed. This entails a progressive decrease of the combustion products conversion into syngas that occurs mainly in the char layer. As will be clear in the next session, this evolution of the process has a direct impact on the "*energy quality*" of the generate $\dot{m}_s$, i.e. on the decrease of its *LHV*. Furthermore, the progressive establishment of the combustion regime leads to an increase of volatile ash particles and particulate matter. The combined effects of high $\dot{V}_{a,wb}$ values and the consequent reduction of the char layer acting also as a filter, leads to a progressive dragging/fluidization regime of particulate matter and ash. This behaviour, compromising the stability of the biomass loss measurement, limits the choice of the maximum acceptable values for $\dot{V}_{a,wb}$ that, in this study, set at 25 and 30 Nl·min^{-1} for *WP* and *TP* respectively. These questions would deserve to be analysed more in depth. Since this is not the primary purpose of this work, reference is made to the following works [81–83] specifically dedicated to evaluate the impact of high $\dot{V}_{a,wb}$ on the propagation rate of the pyrolysis front. The conclusions formulated here do not take into account that the measurements are influenced by errors due to the accuracy of the instruments used. To avoid burdening this discussion, these issues are addressed within the statistical analysis proposed in paragraph 6. As reported, the progressively reduced quantity of char introduces significant errors to the point that a description based solely on the reported measurements can prove to be partially unreliable.

Alongside these observations, a further interesting elaboration can be proposed starting from the overall mass balance, Eq. (4), and substituting the $\dot{m}_{ogp}$ and $\dot{m}_{char}$ terms as expressed by Eqs. (1) and (2) respectively.

Eq. (4) can be rewritten in the following form:

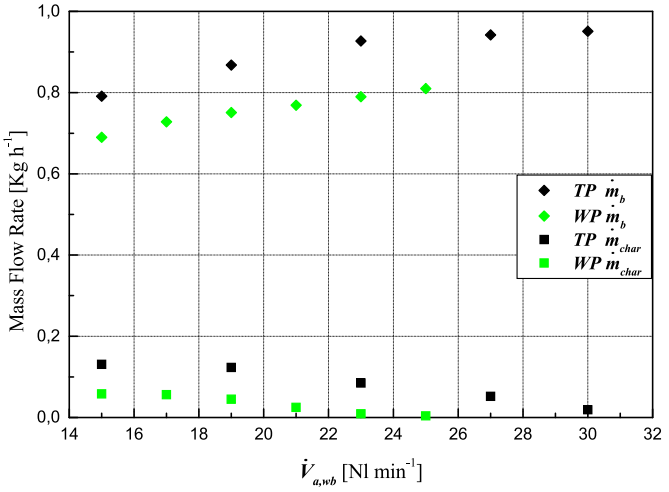

Fig. 5. $\dot{m}_b$ and $\dot{m}_{char}$ trends for *WP* and *TP* Vs. $\dot{V}_{a,wb}$.

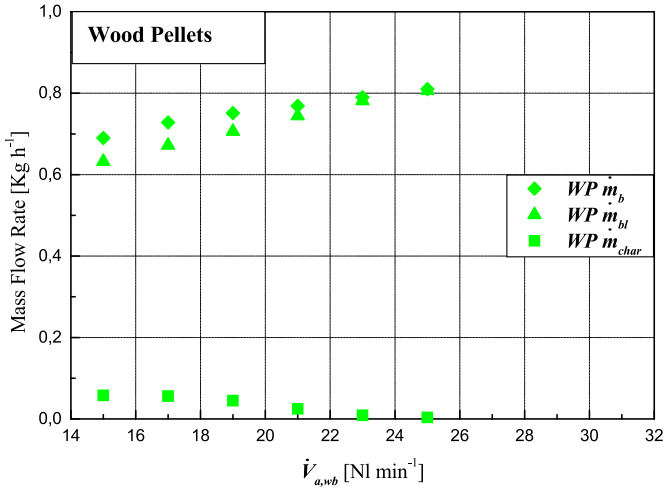

Fig. 6a. $\dot{m}_b$, $\dot{m}_{bl.}$ and $\dot{m}_{char}$ for *WP* Vs. $\dot{V}_{a,wb}$

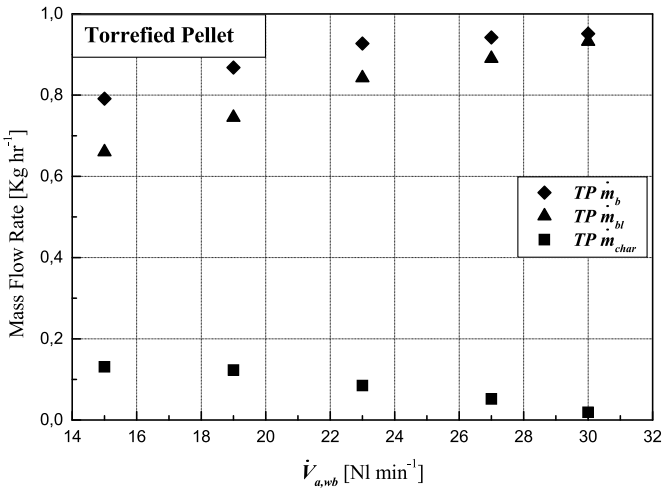

Fig. 6b. $\dot{m}_b$, $\dot{m}_{bl}$ and $\dot{m}_{char}$ for *TP* Vs. $\dot{V}_{a,wb}$

$$\frac{\dot{m}_b}{\dot{m}_{bl}} = \left(1 + \frac{m_{char}}{m_b}\right) \tag{20}$$

Referring to the assumption introduced in Eq. (2), the ratio ($m_{char}/\ m_b$) can be substituted with the ration $\dot{m}_{char}/\ \dot{m}_b$, Eq. (20) can be rearranged to provide an alternative to determine the $\dot{m}_{bl}$:

$$\dot{m}_{bl} = \frac{\dot{m}_b}{\left(1 + \frac{\dot{m}_{char}}{\dot{m}_b}\right)} \tag{21}$$

This equation allows to determine the $\dot{m}_{bl}$ by the knowledge of the $\dot{m}_b$ feeding the gasifier, usually available, and of the unloaded $\dot{m}_{char}$. Once these quantities are determined, it is possible to estimate the $\dot{m}_{ogp}$ through Eq. (1). Trends depicted of previous Figs. (6a,6b) can also be reconsidered by evaluating the impact that the $\dot{m}_b$ has on $\dot{m}_{ogp}$ and, consequently, on $\dot{m}_s$. This clearly emerges from the following Fig. (7) which depicts the $\dot{m}_{ogp}$ Vs. $\dot{m}_b$ highlighting, with solid symbols, the three tests involving *WP* and *TP* carried out at the same $\dot{V}_{a,wb}$.

This representation integrates the contents of previous Fig. (4) concerning $\dot{m}_s$ or $\dot{m}_{ogp}$ quantities as follows: by working at the same $\dot{V}_{a,wb}$, Figs. (4,7), an almost similar amount of $\dot{m}_{ogp}$ ($\dot{m}_s$) can be obtained both from *WP* and *TP* but, from Fig. (7), it emerges that for *TP* this implies the increase of $\dot{m}_b$; from a different point of view, at the same $\dot{m}_b$, the gasifier

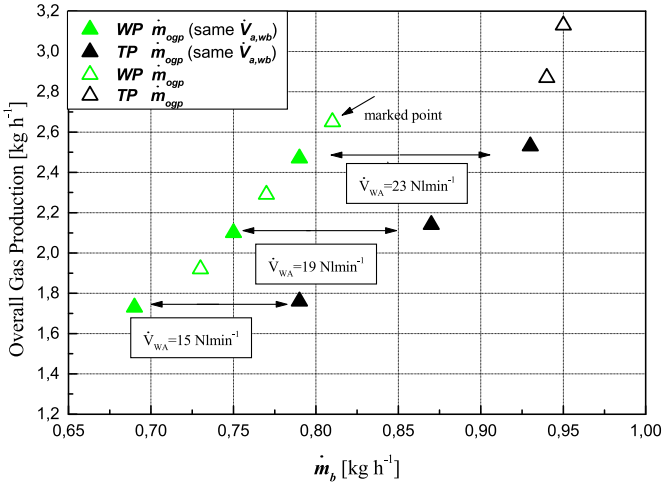

Fig. 7. $\dot{m}_{ogp}$ Vs. $\dot{m}_b$ for *WP* and *TP*. Solid symbols refer to tests carried out at the same $\dot{V}_{a,wb}$.

working with *WP* produces a higher quantity of $\dot{m}_{ogp}$ with respect to that obtained by using *TP,* a condition that is achieved for higher values of $\dot{V}_{a,wb}$. The process involving *TP*, for which the performances seem worse than using *WP* (higher $\dot{m}_b$ to produce similar $\dot{m}_{ogp}$ at the same $\dot{V}_{a,wb}$), has the advantage to be able to work at higher values of $\dot{m}_b$ with respect to *WP* producing, correspondingly, increasing $\dot{m}_{ogp}$ ($\dot{m}_s$). For the case of *WP,* it is important to observe that the limitation is not dictated by a limit value of $\dot{m}_b$ but by the constraint imposed by the maximum acceptable value of $\dot{V}_{a,wb}$ that, for the so design reactor, sets below the maximum one (marked with ← symbol), in Fig. (7) for $\dot{V}_{a,wb}$ = 25 Nl·min^{-1}). As mentioned above discussing about Fig. 6a and b, this is due to the condition that, for *WP*, the $\dot{m}_{char}$ is close to zero even for $\dot{V}_{a,wb}$ values lower than 23 Nl·min^{-1}.

The following Fig. (8) reports the concentration trends of *tars* in the obtained syngas ($\dot{m}_{tars\rightarrow ogp}/\ \dot{V}_s$) and the *tars* to biomass ratio ($\dot{m}_{tars\rightarrow ogp}/\ \dot{m}_b$) both for *WP* and *TP*. This plot highlights that, within the common range of $\dot{V}_{a,wb}$: 15–23 Nl·min^{-1}, the concentration profiles present a similar trend for both biomasses with a minimum reached in correspondence to the same value of $\dot{V}_{a,wb}$ = 19 Nl·min^{-1}. Within this $\dot{V}_{a,wb}$ range, the difference of *tars* concentration between the two biomasses decreases with the increasing of $\dot{V}_{a,wb}$ while, beyond this range, this difference seems to diverge significantly. However, it must be observed that, due the limited number of experimental data, it becomes difficult to recognize a reasonable trend as emerges for the other quantities. Due to these *tars* concentration trends and the results of $\dot{m}_b$ previously discussed, the resulting profiles of the ratio $\dot{m}_{tars\rightarrow ogp}/\ \dot{m}_b$, included in the same figure, represent an expected trend. It is important to observe that, at the same $\dot{V}_{a,wb}$, this ratio reaches lower values for *TP* than for *WP*. This is due to the higher value of the $\dot{m}_b$ in correspondence to the same $\dot{V}_{a,wb}$ and not to an intrinsic characteristic of the torrefied biomass. Indeed, as evidenced in Table 5, for tests involving the same $\dot{V}_{a,wb}$, the $\dot{m}_{tars\rightarrow ogp}$ is practically the same for the two biomass species.

5.2. Energy balance results

The plots proposed in this section depict the trends of the energy parameters introduced in paragraph 4.2. To make the discussion clearer, the results are presented according to an appropriate sequence of topics.

- *Gasification Reactor Power* (P_{gr}) *and Power to Biomass Yield* (Y_{pb}).

The following Fig. (9) reports the trends of the P_{gr} and Y_{pb} quantities Vs. $\dot{V}_{a,wb}$. At the same $\dot{V}_{a,wb}$, the P_{gr} present higher values for *TP* than for *WP* with an increasing trend for both P_{gr} and Y_{pb} as $\dot{V}_{a,wb}$ increases. For

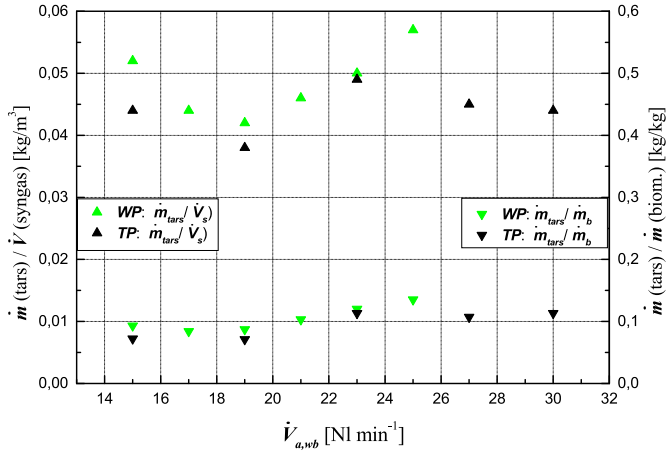

Fig. 8. Tars concentration and tars/biomass ratio for *WP* and *TP* Vs. $\dot{V}_{a,wb}$

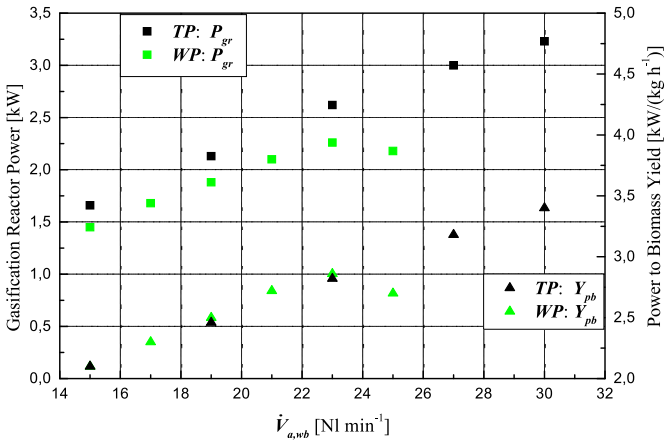

Fig. 9. P_{gr} and Y_{pb} trends for *TP* and *WP* Vs. $\dot{V}_{a,wb}$

both these quantities, the *WP* trend presents a maximum achieved in correspondence to $\dot{V}_{a,wb} = 23$ Nl·min^{-1}. It is interesting to note that at low $\dot{V}_{a,wb}$ values, while the Y_s parameter referred to *TP* performs worse with respect to those achieved for *WP* (see data of Table 5), within low $\dot{V}_{a,wb}$ range the Y_{pb} parameter reaches similar results for both biomasses (Fig. 9).

- *Syngas Low Heating Value (LHV) trends.*

The P_{gr} results can be better understood when they are correlated to the corresponding ones pertaining to *LHV* as proposed in Fig. (10). Over the entire $\dot{V}_{a,wb}$ range, the *LHV* reaches higher values for *TP* than for *WP*. For both biomass, a maximum is observed for LHV, for *TP* in correspondence to slightly higher values of $\dot{V}_{a,wb}$.

Beyond the maximum, the *LHV* of syngas obtained from *WP* decreases more rapidly than that from *TP,* which entails a corresponding decrease of the P_{gr} profile within the $\dot{V}_{a,wb}$ range 23–25 Nl·min^{-1}. For *TP*, the slight decrease of *LHV* beyond the maximum is, however, offset by the continuous increase of $\dot{m}_s$ also at higher $\dot{V}_{a,wb}$ (Fig. 4) which, at the end, entails an increasing trend of P_{gr}. On the next point the discussion will therefore be focused on the analysis of the results of the *LHV* trends. Due to the very similar value observed for $\dot{m}_s$ at the same $\dot{V}_{a,wb}$ values (Figs. 4), Fig. 10 clearly shows that the higher values of P_{gr} achieved for *TP* than for *WP* is clearly due to the contribution of the *LHV*.

- *Syngas Low Heating Value (LHV) analysis*

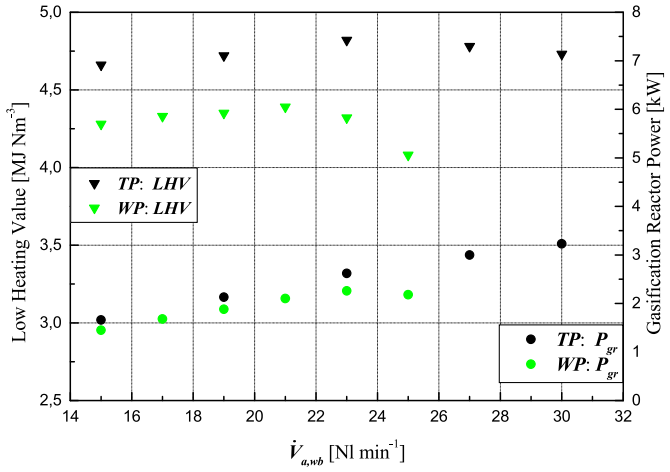

Fig. 10. P_{gr} and *LHV* trends for *TP* and *WP* Vs. $\dot{V}_{a,wb}$.

Fig. (11) depicts the molar fractions trends for CO, H_2 and CH_4 compounds Vs. $\dot{V}_{a,wb}$ monitored in correspondence of the line exiting the gasifier after the traps (Fig. 3). The plotted values, included in Table 6, are the average of the x_{co}, x_{H_2} and x_{CH_4} molar fractions recorded during each test and are implemented in Eq. (15) to calculated the *LHV* of the syngas. For CO and, to a lesser extent, for CH_4, the trends are practically overlapping up to $\dot{V}_{a,wb}$ equal to 19 and 23 Nl·min^{-1} for *WP* and *TP* respectively. Regarding CO, its trend increases continuously for *TP* while, for *WP*, it reaches the maximum of $x_{co} = 18{,}37$ % for $\dot{V}_{a,wb} = 23$ Nl·min^{-1}. For *WP*, the maximum for $x_{H_2} = 14{,}48$ % is achieved around 20–21 Nl·min^{-1} and, all over the $\dot{V}_{a,wb}$ range, its trend sets below that achieved by *TP*. For both species, within the higher ranges of $\dot{V}_{a,wb}$ the x_{H_2} profile decreases, more rapidly for *WP*. The contribution of these three compounds leads to the *LHV* trends highlighted by the continuous lines conferring, thereby, to the syngas obtained from *TP*, a "*higher energy*" quality compared to that generated from *WP*. A more in-depth analysis on the evolution of the obtained *LHV* trends is proposed in the next point.

- *Impact of char on LHV*

At this point of the discussion it seems of some interest to resume what was proposed in section 6.1 regarding the evolution of the $\dot{m}_{char}$ as function of the $\dot{V}_{a,wb}$, a topic discussed as a commentary on Figs. (6a, 6b). The following Fig. (12) integrates the graphs now cited, in the sense that it highlights the impact that the evolution of the char layer has, not only in the resulting mass flow rates trends ($\dot{m}_{bl}$, $\dot{m}_b$: Fig. 6a and b) but, in a more relevant way, in enhancing the energy content of the syngas, i.e. in the evolution of the its *LHV*.

Fig. (12) highlights how the trend of CO is correlated to the evolution of the layer of *char* (in this figure normalized with respect to the biomass charge) through which the combustion products are converted into syngas mainly due to the *Boudouard* and *Carbon steam reforming* reactions, Table 2. It is interesting to note that the x_{co} profile referred to *TP* increases also at higher values of $\dot{V}_{a,wb}$ due to the presence of a layer of char still active, unlike what happens for *WP* for which the x_{co} starts to decrease due to significant reduction or absence of the char layer in correspondence to the higher $\dot{V}_{a,wb}$ range acceptable for this biomass. For *TP* this contributes to limits the decrease of its *LHV* with respect to what happens for the case of the syngas generate from *WP,* as depicted in previous Fig. (11).

- *Carbon Conversion* (η_{CC}) and *Cold Gassification* (η_C) *Efficiencies*

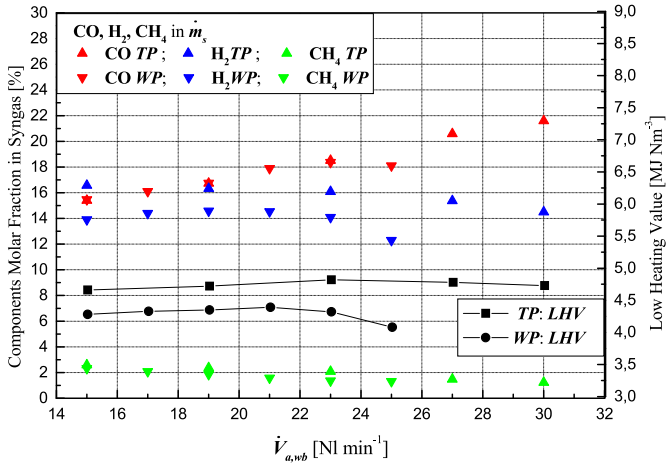

Fig. 11. CO, H_2 and CH_4 molar fraction profiles and syngas *LHV* obtained from *TP* and *WP* Vs. $\dot{V}_{a,wb}$.

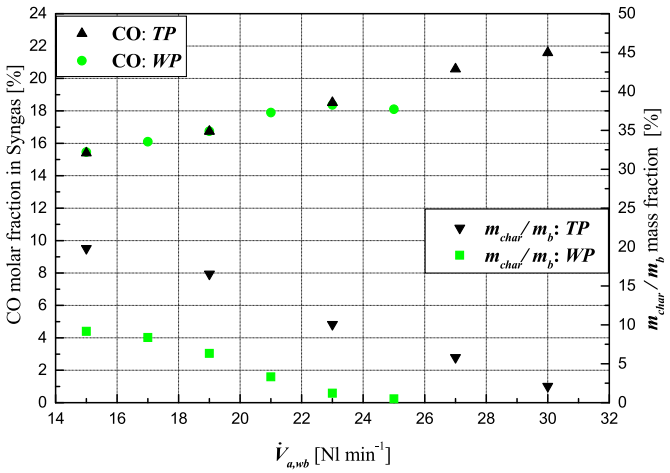

Fig. 12. *Char* % trend and corresponding x_{co} profile Vs. for *TP* and *WP*.

The following Fig. (13), showing the trends of the two parameters: η_{CC} and η_C, represents a synthesis of the discussions carried out so far in presenting the previous diagrams. Considering the η_C, this diagram highlights how, although the P_{gr} values are more performing for *TP* than for WP (Fig. 9), the resulting η_C trend is worse within the lower $\dot{V}_{a,wb}$ range compared to *WP*. Considering Eq. (18), this is explained by the effect of the increase of the $\dot{m}_b$ required to achieve similar gaseous production at the same $\dot{V}_{a,wb}$ (Fig. 7) and to the higher *LHV* of this type of biomass (Table 1). On the other hand, at high flow rates, the η_C reaches a maximum for *WP* while, for *TP,* it continues to grow. A similar trend is observed for the η_{CC} parameters.

6. Statistical analysis

Making reference to Eqs. (1)–(5), the elaboration proposed in this work requires, as input data, the values of $\dot{m}_{bl}$ and $\dot{m}_{char}$ quantities. The $\dot{m}_{bl}$ is determined by monitoring the biomass loss during each test, while $\dot{m}_{char}$ is calculated through Eq. (2) knowing the amount of char (m_{char}) measured at the end of each test. The tests carried out during this study, given the operational complexity, have not been repeated. Therefore, data reported in the manuscript relate to the individual measurements taken during each test. Therefore, the error of the measurements of $\dot{m}_{bl}$ and m_{char} can only be calculated with respect to the accuracy of the utilized scales (10^{-3} kg for the scale used for $\dot{m}_{bl}$; 10^{-4} kg for that of m_{char}), while systematic and random errors cannot evidently be considered. The following Figs. 14 and 15 reports the trends of the accuracy error bars % (in percentage to enhance the vision of bars) for $\dot{m}_{bl}$ and m_{char} quantities. While for $\dot{m}_{bl}$ the errors trends are comparable and almost constant for *WP* and *TP* over the entire $\dot{V}_{a,wb}$ range, for m_{char} the difference increases due to the rapid extension of the error bars following the decrease of char amount that tends to 0 as $\dot{V}_{a,wb}$ increases, as described in sub-section 5.2: *Impact of char on LHV*. Fig. (15) highlights that, at high values of $\dot{V}_{a,wb}$, the measurements of m_{char}, and consequently of $\dot{m}_{char}$, present an unacceptable accuracy error as evidenced by the negative value of the bars, a condition that becomes particularly evident for *WP*. This means that the conclusions reported in the cited paragraph on the importance of the char layer in characterizing the "*quality*" of syngas, deduced by considering only the measurement trends, as emerges from this analysis have to be understood as a "*qualitative*" trend, while a definitive quantitative assessment would require repeated measurements taken using high-precision instruments.

Despite the criticality due to the limited number of experimental data, the Standard Deviation (St. Dev.) value has been calculated in any case for each of the quantities addressed in the introduced procedure. The results are reported in the following Tables 7 and 8 for mass flow rate quantities and energy parameters respectively. In addition, the corresponding St. Dev. trends are depicted in Figs. 16 and 17. It is to observe that, in this context, these trends do not indicate how much the data of a distribution deviate from the average value. Since, for a selected quantity, each data is referred to different conditions (different $\dot{V}_{a,wb}$, Figs. 14 and 15), the average values reported in these Tables are not, rigorously, actual '*average*' values. Therefore, the St. Dev. bars trends reported in Figs. 16 and 17 do not account for the deviation errors of the data as usual, but an indication of the *distribution,* with respect to $\dot{V}_{a,wb}$, of the experimental measurements of a quantity around the "*average*" value. As general outcome, these diagrams provide an immediate comparative view of the explained St. Dev. distribution between *TP* and *WP* for each of the reported quantities. In details, Fig. (16) highlights the small distribution range for quantities as $\dot{m}_{bl}$, $\dot{m}_b$ and $\dot{m}_{char}$ whose result can be traced back to the mass balances involving only solid (biomass) quantities, Eqs. (2) and (3). Quantities as $\dot{m}_{ogp}$, $\dot{m}_s$ and Y_s are determined by solving the mass balance, Eqs. (1), (7) and (8), including the contribution of mass or volumetric air flow rate. This makes it clear how the growing trends of $\dot{m}_{ogp}$ and $\dot{m}_s$ with $\dot{V}_{a,wb}$, Fig. (4), are mainly due the contribution of the air amount than that of the gasification of the solid quantities that, moreover, remains limited. The St. Dev. range for the power parameter P_{gr} is, correspondingly, the higher one within the Energy indexes, Fig. (17), since it accounts for the relevant distribution range of $\dot{m}_s$ that, in turn, is mainly due to that of the $\dot{V}_{a,wb}$. The St. Dev. range of LVH is not very different for *WP* and *TP*

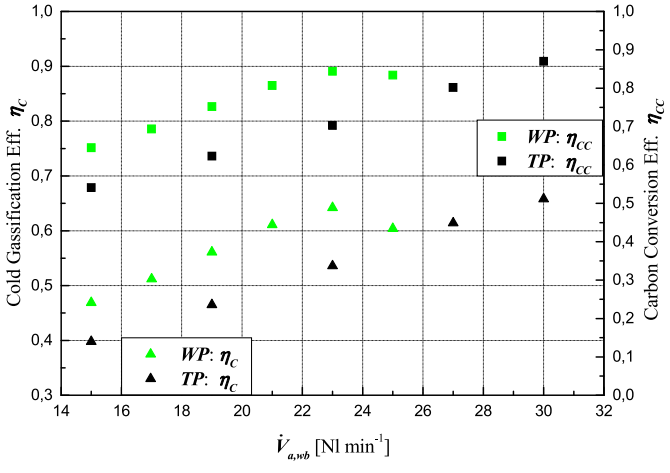

Fig. 13. η_C and η_{CC} trends for *WP* and *TP* Vs. $\dot{V}_{a,wb}$.

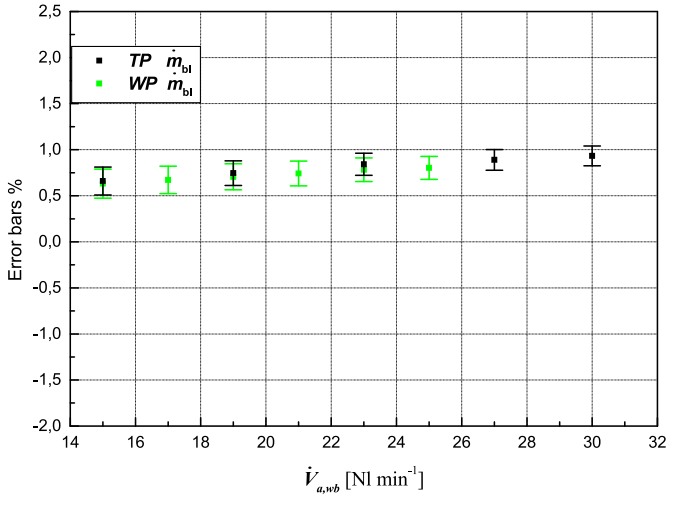

Fig. 14. Accuracy error bars % trends of $\dot{m}_{bl}$ for *WP* and *TP* Vs. $\dot{V}_{a,wb}$.

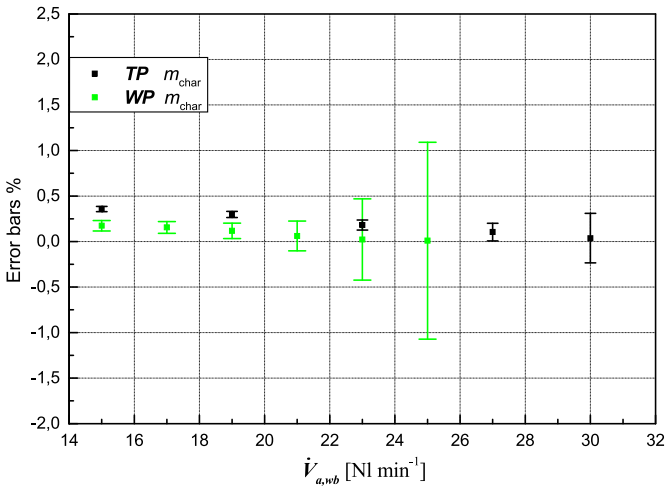

Fig. 15. Accuracy error bars % trends of m_{char} for *WP* and *TP* Vs. $\dot{V}_{a,wb}$.

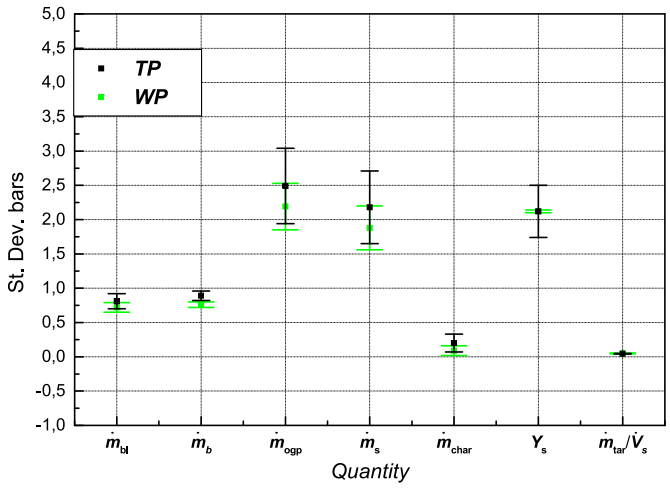

Fig. 16. St. Dev. distribution bars for quantities referred derived from mass balance.

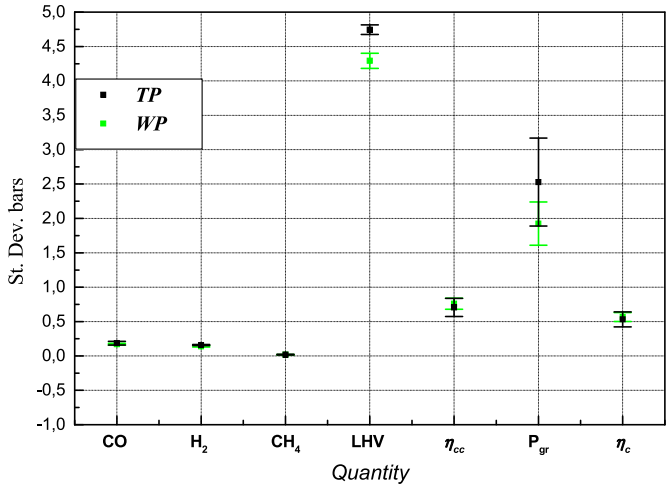

Fig. 17. St. Dev. distribution bars for quantities derived from energy balance.

(Fig. 17), but the higher average value of both *LHV* and $\dot{m}_s$ for the *TP* contributes to set the distribution range of P_{gr} at higher values for *TP* than *WP*.

7. Limits of the proposed experimental procedure

The most significant criticality found in this experimentation lies in the fact that, due to the complexity of the tests to be performed, the measurements were not repeated. The availability of data, while providing interesting insights on the emerging issues, is therefore limited. A statistical elaboration has been proposed, but the results cannot be widely utilized to obtain further reliable trends. Some conclusions, based solely on direct measurements and not supported by statistical information, have to be critically accepted. This should be particularly accounted for measurements made by imposing high air flow rates, for which the data for char amount is affected by substantial inaccuracies.

From a methodological point of view, the work does not propose, at this step, a comparison between the proposed calculation procedure, defined for a batch configuration, and the experimental results obtained from the exercise of a continuous reactor. This would provide an independent experimental feedback on the effective reliability of the proposed method. In addition to this, a further limitation is made up by the small size of the adopted batch prototype, which does not allow to extend the air flow rates to a wider range of experimental conditions, currently limited. From an operational point of view, it would be appropriate to integrate or develop, through models, the problems related to the onset of the fluidization regime that occurs at high air flow rates. This is a critical aspect because it affects the amount of char present in the reactor that could be removed, due to the presence of fluidization effects, reducing so that its functionality.

Table 7
Average and Standard Deviation for *WP* and *TP* quantities derived from mass balance.

Quantities derived from mass balance [kg·h^{-1}]														
	$\dot{m}_{bl}$		$\dot{m}_{ogp}$		$\dot{m}_s$		$\dot{m}_{char}$		$\dot{m}_b$		Y_s [Nm^3·kg^{-1}]		$\dot{m}_{tars}/\dot{V}_s$ [kg·Nm^{-3}]	
	WP	***TP***	***WP***	***TP***	***WP***	***TP***	***WP***	***TP***	***WP***	***TP***	***WP***	***TP***	***WP***	***TP***
Aver.	0.723	0.812	2.193	2.486	1,882	2,182	0.033	0.082	0.757	0.894	2.123	2.116	0.049	0.044
St.Dev.	0.067	0.111	0.344	0.550	0.316	0.528	0.024	0.047	0.043	0.065	0.252	0.383	0.006	0.004

Table 8
Average and Standard Deviation values for composition and energy parameters of *WP* and *TP*.

Syngas composition and energy parameters														
	x_{CO}		x_{CH_4}		x_{H_2}		*LHV*		η_{CC}		P_{gr}		η_C	
	WP	***TP***	***WP***	***TP***	***WP***	***TP***	***WP***	***TP***	***WP***	***TP***	***WP***	***TP***	***WP***	***TP***
Aver.	0.171	0.186	0.017	0.019	0.140	0.158	4.292	4.745	0.760	0.706	1.925	2.528	0.566	0.532
St.Dev.	0.012	0.026	0.004	0.006	0.009	0.008	0.110	0.070	0.081	0.133	0.315	0.640	0.065	0.109

8. Conclusions

This paper presents the results of an innovative experimental elaboration applied to mass and energy balances of a pilot plant batch gasifier using air as gasification agent and working with raw and torrefied biomass densified in form of pellet. The novelty consists in the continuous monitoring of the biomass loss by exploiting the steady-state conditions detected during the process evolution. By using as input variables: the air flow rate, suitable chosen within a define range, and the char flow rate, estimated from the measurements of the overall char production amount, all the mass flow rates quantities involved in the process have been determined as if they accord to those of a continuous updraft fixed-bed gasifier configuration. By including the monitoring of the composition of the syngas compounds, the performances of the energy quantities have been calculated as well. As important outcome, the proposed approach demonstrates the relevant role of airflow rate as guiding parameter from which depends the optimal achievements of the process.

Additionally, this work confirms the increasing performances of the process powered by torrefied biomass, although the optimal ones are achieved for higher mass flow rate than those required using raw biomass. The results emerging from this research look promising to improve the design and control procedures of biomass gasifier and to consolidate the potentialities of biomass exploitation within the current renewable energy scenarios.

CRediT authorship contribution statement

M. Grigiante: Methodology, Investigation, Conceptualization. **D. Antolini:** Software, Data curation.

Declaration of competing interest

The authors declare that they have no known competing financial interests or personal relationships that could have appeared to influence the work reported in this paper.

Data availability

Data will be made available on request.

References

[1] Ferreiro AI, Ferreira AF, Fernandes EC, Coelho P. Influence of process parameters on biomass gasification: a review of experimental studies in entrained flow reactors and droptube furnaces. Biomass Bioenergy 2024;185:107217.
[2] Yan R, Zhou Z, Fu Y, Wang R, Cai L. Thermodynamic, economic, and environmental analysis of a biomass gasification power plant based on the Allam cycle. Energy 2025;314:134105.
[3] Zhang Y, Hou D, Sun X, Zhu X, Yan B, Chen G. Different pretreatment of biomass for gasification: a critical review. J Energy Inst 2025;119:101992.
[4] Goel A, Moghaddam EM, Liu W, He C, Konttinen J. Biomass ,looping gasification for high-quality syngas: a critical review and technological outlooks. Energy Convers Manag 2022;268:116020.
[5] Yuksel YE, Ozturk M, Dincer I. Development and assessment of a biomass-gasification based multigenerational plant for production of hydrogen and ammonia fuels. Fuel 2025;380:133187.
[6] Situmorang YA, Zhao Z, Yoshida A, Guan G. Small-scale biomass gasification systems for power generation (< 200 kw class). Renew Sustain Energy Rev 2020; 117:109486.
[7] Indrawana N, Kumarb A, Molierec M, Sallamd KA, Huhnkeb RL. Distributed power generation via gasification of biomass and municipal solid waste: a review. J Energy Inst 2020;93:2293–313.
[8] Peng W, Chen H, Liu J, Zhao X, Xu G. Techno-economic assessment of a conceptual waste-to- energy CHP system combining plasma gasification, SOFC, gas turbine and supercritical CO_2 cycle. Energy Convers Manag 2021;245. 116020: 114622.
[9] Yang S, Wang G, Liu Z, Deng C, Xie N. Energy, exergy and exergo-economic analysis of a novel SOFC based CHP system integrated with organic Rankine cycle and biomass cogasification. Int J Hydrogen Energy 2024;53:1155–69.
[10] Abouemara K, Shahbaz M, Mckay G, Al-Ansari T. The review of power generation from integrated biomass gasification and solid oxide fuel cells: current status and future directions. Fuel 2024;360:130511.
[11] Pimentela FS, dos Santos BF, Pradellea F. Investigation of artificial neural network topologies to predict biomass gasification and comparison with a thermodynamic equilibrium model. Energy 2024;308:132762.
[12] Du J, Zou Y, Dahlak A. Process development and multi-criteria optimization of a biomass gasification unit combined with a novel CCHP model using helium gas turbine, kalina cycles, and dual-loop organic flash cycle. Energy 2024;391:130319.
[13] Gao K, Chen G, Yan B, Ti S, Wang H, Si G, Qi T. Modeling of biomass thermal decomposition/gasification in a downdraft gasifier under low pressure by Aspen plus. Therm Sci Eng Prog 2025:103229.
[14] Song H, Xia J, Hu Q, Cheng W, Yang Y, Chen H, Yang H. Comprehensive experimental assessment of biomass steam gasification with different types: correlation and multiple linear regression analysis with feedstock characteristics. Renew Energy 2024;237:121649.
[15] Li H, Liu X, Cao B, Liuc C, Yanga J, Chen W. Optimisation of downdraft gasifier in biomass-fuelled power generation system: experimental analysis and chemical kinetics modelling with tar cracking. Energy 2024;313:133924.
[16] Nunes LJR, Leonor C, Casau M, Dias MF, Matias JCO, Teixeira LC. Agroforest woody residual biomass-to-energy supply chain analysis: feasible and sustainable renewable resource exploitation for an alternative to fossil fuels. Results Eng 2023; 17:101010.
[17] Tan Z, Zeng X, Lin B. How do multiple policy incentives influence investors' decisions on biomass co-firing combined with carbon capture and storage retrofit projects for coal-fired power plants? Energy 2023;278:127822.
[18] Singh A, Christensen T, Panoutsou C. Policy review for biomass value chains in the European bioeconomy. Global Transitions 2021;3:13–42.
[19] Perera SMHD, Wickramasinghe C, Samarasiri BKT, Narayana M. Modeling of thermochemical conversion of waste biomass-a comprehensive review. Biofuel Res. J. 2021;8:1481–528.
[20] Kaygusuz K. Climate change and biomass energy for sustainability, energy sources part B econ plan. Pol. 2010;5:133–46.
[21] Bilgilia F, Koçakb E, Bulutc Ü, Kuşkayad S. Can biomass energy be an efficient policy tool for sustainable development? Renew Sustain Energy Rev 2017;71: 830–45.
[22] https://www.iea.org/topics/renewables/subtopics/bioenergy/.
[23] Santos SM, Assis AC, Gomes L, Nobre C, Brito P. Waste gasification technologies: a brief overview. Waste 2023;1:140–65.
[24] Tezer O, Karaba N, Ongen A, Çolpan CO, Ayol A. Biomass gasification for sustainable energy production: a review. Int J Hydrogen Energy 2022;47: 15419–33.
[25] Erdiwansyah Gani A, Yana S, Zaki M, Sarjono RE. Analysis of technological developments and potential of biomass gasification as a viable industrial process: a review. Case Stud Chem Environ Eng 2023;8:100439.
[26] Li H, Liu X, Cao B, Liu C, Yanga J, Chen W. Optimisation of down draft gasifier in biomass- fuelled power generation system: experimental analysis and chemical kinetics modelling with tar cracking. Energy 2024;313:133924.
[27] Tian H, Li R, Zhu Y. Blend of flue gas from a methane-fueled gas turbine power plant and syngas from biomass gasification process to feed a novel trigeneration application: thermodynamic-economic study and optimization. Energy 2023;285: 129425.
[28] Osat M, Shojaati F, Osat M. Techno-economic assessment of butanol and pentanol productions from sorption enhanced chemical looping gasification of a lignocellulosic biomass. Renew Energy 2023;217:119176.
[29] Basu P. Biomass gasification, pyrolysis and torrefaction. Practical design and theory. second ed. Academic Press; August 13, 2013.
[30] Pio DT, Tarelho LAC, Pinto PCR. Gasification-based biorefinery integration in the pulp and paper industry: a critical review. Renew Sustain Energy Rev 2020;133: 110210.
[31] Singh Siwal S, Zhang Q, Sun C, Thakur S, Kumar Gupta V, Kumar Thakur V. Energy production from steam gasification processes and parameters that contemplate in biomass gasifier – a review. Bioresour Technol 2020;297:122481.
[32] Heredia AJA, Guillen R. Composition of plant cell walls. Eur Food Res Tech 1995; 200:24–31.
[33] Mansor AM, Shiun LJ, Ani FN, Haslenda H, Ho WSH. Characteristics of cellulose, hemicellulose and lignin of MD2 pineapple biomass. Chem Eng Tran 2019;72.
[34] Wang S, Dai G, Ru B, Zhao Y, Wang X, Xiao G, Luo Z. Influence of torrefaction on the characteristics and pyrolysis behavior of cellulose. Energy 2017;120:864–71.
[35] Chen WH, Lin YY, Chu YS, Ubando AT, Show PL, Ong HC, Chang JS, Ho SH, Culaba AB, Petrissans A, Petrissans M. Progress in biomass torrefaction: principles, applications and challenges. Prog Energy Combust Sci 2021;82:100887.
[36] Di Marcello M, Tsalidis GA, Spinelli G, De Jong W, Kiel JHA. Pilot scale steam-oxygen CFB gasification of commercial torrefied wood pellets. The effect of torrefaction on the gasification performance. Biomass Bioenergy 2017;105:411–20.
[37] Adeleke AA, Ikubanni PP, Emmanuel SS, Fajobi OM, Nwachukwu P, Ademidun A, Adesibikan AA, Odusote JK, Adeyemi EO, Abioye OM, Okolie JA. A comprehensive review on the similarity and disparity of torrefied biomass and coal properties. Renew Sustain Energy Rev 2024;199:114502.
[38] Chen WH, Lin BJ, Lin YY, Chu YS, Ubando AT, Show PL, Petrissans M. Progress in biomass torrefaction: principles, applications and challenges. Prog Energy Combust Sci 2021;82:100887.
[39] Thengane SK, Kung KS, Gomez-Barea A, Ghoniem AF. Advances in biomass torrefaction: parameters, models, reactors, applications, deployment, and market. Prog Energy Combust Sci 2022;93:101040.
[40] Nunes LJR. Torrefied biomass as an alternative in coal-fueled power plants: a case study on grindability of agroforestry waste forms. Clean Technol 2020;2:270–89.

[41] Zheng J, Zhang H, Gong X, Zhang Y. The integration of biomass torrefaction with coal gasification: performance study and process simulation. J Anal Appl Pyrolysis 2024;180:106559.
[42] Chen W, Peng J, Bi XT. A state-of-the-art review of biomass torrefaction, densification and applications. Renew Sustain Energy Rev 2015;44:847–66.
[43] Adeleke AA, Odusote JK, Ikubanni PP, Lasode OA, Malathi M, Paswan D. Essential basics on biomass torrefaction, densification and utilization. Int J Energy Res 2021; 45:1375–95.
[44] Chen L, Wen C, Wang W, Liu T, Liu E, Liu H, Li Z. Combustion behaviour of biochars thermally pretreated via torrefaction, slow pyrolysis, or hydrothermal carbonisation and co fired with pulverised coal. Renew Energy 2020;161:867–77.
[45] Agar AD, Rudolfsson M, Lavergne S, Melkior T, Da Silva Perez D, Dupont C, Campargue M, Kalen G, Larsson SH. Pelleting torrefied biomass at pilot-scale. Quality and implications for co-firing. Renew Energy 2021;178:766–74.
[46] Kuttin KW, Yu H, Yanga M, Ding L, Chen X, Yu G, Wang F. Experimental and numerical modeling of carbonized biomass gasification: a critical review. Green Carbon 2024;2:176–96.
[47] Zhou Q, Shen Y, Gu X. Progress in torrefaction pretreatment for biomass gasification. Green Chem 2024;26(18):9652–70.
[48] Dudyński M, Van Dyk JC, Kwiatkowski K, Sosnowska M. Biomass gasification: influence of torrefaction on syngas production and tar formation. Fuel Process Technol 2015;131:203–12.
[49] Rudolfsson M, Wolfgang Stelte W, Lestander TA. Process optimization of combined biomass torrefaction and pelletization for fuel pellet production – a parametric study. Appl Energy 2015;140:378–84.
[50] Hu Q, Yang H, Xu H, Wu Z, Lim CJ, Bi XT, Chen H. Thermal behavior and reaction kinetics analysis of pyrolysis and subsequent in-situ gasification of torrefied biomass pellets. Energy Convers Manag 2018;161:215. 214.
[51] He Z, Sun Y, Cheng S, Jia Z, Tu R, Wu Y, Shen X, Zhang F, Jiang E, Xu X. The enhanced rich H_2 from co-gasification of torrefied biomass and low rank coal: the comparison of dry/wet torrefaction, synergetic effect and prediction. Fuel 2021; 287:119473.
[52] Peng H, Cai W, Huang M, Xia S, Zhu L, Fang X, Ma Z. Advancing biomass gasification by the dry and wet torrefaction pretreatment. Energy 2025;324: 136118.[a] Deng J, Wang GJ, Kuang JH, Zhang YL, Luo YH. Pretreatment of agricultural residues for co- gasification via torrefaction. J Anal Appl Pyrolysis 2009;86:331–7.
[53] Prins MJ, Ptasinski KJ, Janssen FJJG. More efficient biomass gasification via torrefaction. Energy 2006;31:3458–70.
[54] Weiland F, Nordwaeger M, Olofsson I, Wiinikka H, Nordin A. Entrained flow gasification of torrefied wood residues. Fuel Process Technol 2014;125:51–8.
[55] Sarkar M, Kumar A, Tumuluru JS, Patil KN, Bellmer DD. Gasification performance of switchgrass pretreated with torrefaction and densification. Appl Energy 2014; 127:194–201.
[56] Pinto F, Gominho J, Andréa RN, Gonçalvesa D, Miranda M, Varela F, Neves D, Santos J, Lourenço A, Pereira Helena. Improvement of gasification performance of Eucalyptus globulus stumps with torrefaction and densification pre-treatments. Fuel 2017;206:289–99.
[57] ISO 17225-2. Solid biofuels – Fuel specifications and classes – Part 2: Graded wood pellets 2021.
[58] Grigiante M, Antolini D. Mass yield as guide parameter of the torrefaction process. An experimental study of the solid fuel properties referred to two types of biomasses. Fuel 2015;153:499–509.
[59] AOAC method 930. 15. Loss on drying (moisture) for feeds (at 135_C for 2 hours)/ dry matter on oven drying for feed (at 135_C for 2 hours) official methods. Official methods of analysis. seventeenth ed. Gaithersburg, MD: AOAC International; 2000.
[60] DD CEN/TS 14775: solid biofuels. Method for the determination of ash content. British Standards; 2004. p. 12.
[61] Reed TB, Graboski MS, Levie B. Fundamentals development & scale-up of the air-oxygen stratified downdraft gasifier. Biomass Energy Foundation Press; 1994.
[62] Molino A, Chianese S, Musmarra D. Biomass gasification technology: the state of the art overview. J Energy Chem 2016;25(1):10–25.
[63] Umeki K, Häggström G, Bach-Oller A, Kirtania K, Furusjö E. Reduction of tar and soot formation from entrained-flow gasification of woody biomass by alkali impregnation. Energy Fuel 2017;31:5104–10.
[64] Ahmed AMA, Salmiaton A, Choong TSY, Wan Azlina WAKG. Review of kinetic and equilibrium concepts for biomass tar modeling by using Aspen Plus. Renew Sustain Energy Rev 2015;52:1623–44.
[65] Gabbar HA, Lisi D, Aboughaly M, Damideh V, Hassen I. Modeling of a plasma based waste gasification system for solid waste generated on board of typical cruiser vessels used as a feedstock. Designs 2020;4(3):33.
[66] Ren J, Cao JP, Zhao XY, Yang FL, Wei XY. Recent advances in syngas production from biomass catalytic gasification: a critical review on reactors, catalysts, catalytic mechanisms and mathematical models. Renew Sustain Energy Rev 2019;116: 109426.
[67] Sansaniwal SK, Pal K, Rosen MA, Tyagi SK. Recent advances in the development of biomass gasification technology: a comprehensive review. Renew Sustain Energy Rev 2017;72:363–84.
[68] Daugaard DE, Brown RC. Enthalpy for pyrolysis for several types of biomass. Energy Fuel 2003;17(4).
[69] Ramos A, Monteiro E, Rouboa A. Numerical approaches and comprehensive models for gasification process: a review. Renew Sustain Energy Rev 2019;110: 188–206.
[70] Wei J, Wang M, Wang F, Song X, Yu G, Liu Y, Vuthaluru H, Xu J, Xu Y, Zhang H, Zhang S. A review on reactivity characteristics and synergy behavior of biomass and coal Co- gasification. Int J Hydrogen Energy 2021;46(33):17116. e32.
[71] McKendry P. Energy production from biomass (Part 3): gasification technologies. Bioresour Technol 2002;83(1):55–63.
[72] Situmorang YA, Zhao Z, Yoshida A, Kasai Y, Abudula A, Guan G. Potential power generation on a small-scale separated-type biomass gasification system. Energy 2019;179:19–29.
[73] Ondze F, Boutin O, Ruiz JC, Ferrasse JH, Charton F. Supercritical water gasification of beet residues: from batch to continuous reactor. Chem Eng Sci 2015;123:350–8.
[74] Li H, Zhang M, Wang H, Han X, Zeng Y, Xu CC. Comparison study of supercritical water gasification for hydrogen production on a continuous flow versus batch reactor. Bioresour Technol 2024;391:129923.
[75] Ge H, Guo W, Shen L, Song T, Xiao J. Experimental investigation on biomass gasification using chemical looping in a batch reactor and a continuous dual reactor. Chem Eng J 2016;286:689–700.
[76] Jia J, Xub L, Abudula A, Suna B. Effects of operating parameters on performance of a downdraft gasifier in steady and transient state. Energy Convers Manag 2018; 155:138–46.
[77] Lamarche P, Tazerout M, Gelix F, Köhler S, Mati K, Paviet F. Modelling of an indirectly heated fixed bed pyrolysis reactor of wood:transition from batch to continuous staged gasification. Fuel 2013;106:118–28.
[78] Carmona OM, Vederza A, Morales AD, Lenis YA. Steady and transient state behavior of a gasification process under fixed-bed downdraft configuration. Heliyon 2024;10:e34781.
[79] Brandina J, Liliedahlb T. Unit operations for production of clean hydrogen-rich synthesis gas from gasified biomass. Biomass Bioenergy 2011;35:S8–15.
[80] Kaewluan S, Pipatmanomai S. Gasification of high moisture rubber woodchip with rubber waste in a bubbling fluidized bed. Fuel Process Technol 201; 92:671–677..
[81] Yamazaki T, Kozu H, Yamagata S, Murao N, Ohta S, Shiya S. Effect of superficial velocity on tar from downdraft gasification of biomass. Energy Fuels 2005;19: 1186–91.
[82] Garcìa-Bacaicoa P, Mastral JF, Ceamanos JF, Berrueco C, Serrano S. Gasification of biomass/high density polyethylene mixtures in a downdraft gasifier. Bioresour Technol 2008;99:5485–91.
[83] Tinaut FV, Melgar A, Pérez JF, Horrillo A. Effect of biomass particle size and air superficial velocity on the gasification process in a down draft fixed bed gasifier.an experimental and modelling study. Fuel Process Technol 2008;89:1076–89.